NASA CONTRACTOR REPORT

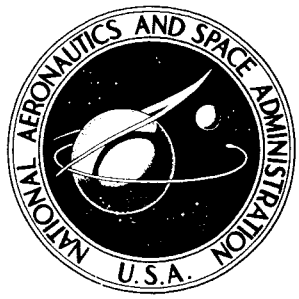

NASA CR-2462

NASA CR-2462

ANALYSIS OF DYNAMIC STALL USING UNSTEADY BOUNDARY-LAYER THEORY

by R. M. Scruggs, J. F. Nash, and R. E. Singleton

Prepared by
SCIENTIFIC & BUSINESS CONSULTANTS, INC.
Atlanta, Ga. 30339
for Langley Research Center

NATIONAL AERONAUTICS AND SPACE ADMINISTRATION • WASHINGTON, D. C. • OCTOBER 1974

1. Report No.	2. Government Accession No.	3. Recipient's Catalog No.
NASA CR-2462		

4. Title and Subtitle	5. Report Date
ANALYSIS OF DYNAMIC STALL USING UNSTEADY BOUNDARY - LAYER THEORY	October 1974
	6. Performing Organization Code

7. Author(s)	8. Performing Organization Report No.
R. M. Scruggs, J. F. Nash, and R. E. Singleton	
	10. Work Unit No.

9. Performing Organization Name and Address	11. Contract or Grant No.
Scientific and Business Consultants, Inc. 9 Perimeter Place, N.W. Atlanta, Georgia 30339	NAS1-11991
	13. Type of Report and Period Covered
12. Sponsoring Agency Name and Address	Contractor Report
National Aeronautics and Space Administration Washington, D.C. 20546	14. Sponsoring Agency Code

15. Supplementary Notes

Final Report - The contract research effort which led to this report was financially supported by USAAMRDL - Langley Directorate.

16. Abstract

The unsteady turbulent boundary layer and potential flow about a pitching airfoil are analyzed using numerical methods to determine the effect of pitch rate on the delay in forward movement of the rear flow reversal point. An explicit finite difference scheme is used to integrate the unsteady boundary layer equations, which are coupled at each instant of time to a fully unsteady and nonlinear potential flow analysis. A substantial delay in forward movement of the reversal point is demonstrated with increasing pitch rate, and it is shown that the delay results partly from the alleviation of the gradients in the potential flow, and partly from the effects of unsteadiness in the boundary layer itself.

The predicted delay in flow-reversal onset, and its variation with pitch rate, are shown to be in reasonable agreement with experimental data relating to the delay in dynamic stall. From the comparisons it can be concluded (a) that the effects of time-dependence are sufficient to explain the failure of the boundary layer to separate during the dynamic overshoot, and (b) that there may be some link between forward movement of the reversal point and dynamic stall.

17. Key Words (Suggested by Author(s))	18. Distribution Statement
Boundary layer, pitching airfoil, unsteady boundary layer, turbulent boundary layer, boundary layer separation, dynamic stall	UNCLASSIFIED - Unlimited Star Category 12

19. Security Classif. (of this report)	20. Security Classif. (of this page)	21. No. of Pages	22. Price*
Unclassified	Unclassified	66	$3.75

*For sale by the National Technical Information Service, Springfield, Virginia 22151

CONTENTS

LIST OF FIGURES

LIST OF FIGURES

SUMMARY

The coupled unsteady turbulent boundary layer and potential flow about a pitching airfoil are analyzed using numerical methods to determine the effect of pitch rate on the delay in forward movement of the rear flow reversal point. An explicit finite difference scheme is used to integrate the unsteady boundary layer equations, which are coupled at each instant of time to a fully unsteady and nonlinear potential flow analysis. A substantial delay in forward movement of the reversal point is demonstrated with increasing pitch rate, and it is shown that the delay results partly from the alleviation of the gradients in the potential flow, and partly from the effects of unsteadiness in the boundary layer itself.

The predicted delay in flow-reversal onset, and its variation with pitch rate, are shown to be in reasonable agreement with experimental data relating to the delay in dynamic stall. From the comparisons it can be concluded (a) that the effects of time-dependence are sufficient to explain the failure of the boundary layer to separate during the dynamic overshoot, and (b) that there may be some link between forward movement of the reversal point and dynamic stall.

SYMBOLS

A,B,C,F	Matrices occurring in the finite difference equations
L	Empirical scale of turbulence function
H_∞	Total head
Q	Total velocity magnitude
U,V	Ensemble average velocities in the s and y-directions
a_1,a_2	Empirical coefficients in the turbulence model
c	Airfoil chord
h	Height of the computation domain
p	Pressure
r	Magnitude of position vector in airfoil coordinates
s	Arc length along the airfoil surface
t	Time
u,v	Fluctuating velocity components
x	Distance measured along airfoil chord
y	Distance measured along a local normal to airfoil surface
Γ	Circulation
α	Angle of attack, in radians unless otherwise noted
β	A parameter in the numerical method
γ	Circulation distribution
δ	Boundary layer thickness
δ^*	Boundary layer displacement thickness
η	Transformed coordinate in the numerical method
ρ	Density
ω	Rotation rate, rad./sec.

φ	Velocity potential
τ	Turbulent shear stress, psi.
τ_w	Turbulent shear stress at the wall divided by ρQ^2

Subscripts

e	Denotes conditions at the edge of the boundary layer
r	Denotes relative motion in an inertial frame of reference

Superscript

$(\overline{\ })$	Denotes a vector or a time or ensemble averaged quantity

ANALYSIS OF DYNAMIC STALL USING UNSTEADY BOUNDARY-LAYER THEORY *

by

R. M. Scruggs, J. E. Nash, R. E. Singleton+

(+ now, Chief, Fluid Mechanics Branch, Army Research Office, Duke Station. Durham, N. C.)

Introduction

The phenomenon of dynamic stall, or delay of the angle of stall due to unsteady motion, has been the subject of intense investigation for several years. There remains some controversy as to the exact mechanisms responsible for the delay, and the extent to which each is responsible. Dynamic stall is identified as a limiting factor in the design of high speed helicopters, and attempts to predict control linkage loads due to it have not met with great success. From the outset, experimental work has proceeded along lines intended to simulate actual flight conditions for a helicopter rotor.(1) From these data, design oriented prediction methods have evolved, and to the extent that test cases represent design conditions of new aircraft, the empirical methods resulting from such tests have generated reasonable design envelope values.(2) It has been demonstrated that three-dimensional effects associated with rotor geometry do not contribute significantly in the onset of stall flutter for a helicopter.(3) It has further been shown that three-dimensional effects associated with the steady turbulent

* The contract research effort which has lead to the results in this report was financially supported by USAAMRDL (Ames Directorate).

boundary layer of the rotor are not of significance in the stall delay phenomenon[4]. These results lend encouragement to the development of a two-dimensional, or quasi two-dimensional, theory capable of predicting dynamic stall and the consequent stall flutter excursions.

Several approaches have been taken in the past to treating dynamic stall. Most have attacked the complete phenomenon, from pre-separation through the circulation loss and return to attached flow. Notable contributions have been made by Ham[5], Carta, et al.[6], Ericsson and Reding[7], Crimi[8], and others. Several methods in present use are predicated on the unsteady aerodynamics of an airfoil oscillating in stall with a prescribed amplitude. Unfortunately most existing experimental data were obtained in this way, with only mild variations in the oscillatory form allowed. It is difficult to isolate the various mechanisms in such data because of history effects in the flow and because dynamic stall is almost certainly dependent on the particular motion of the airfoil before and during the stall break.

A number of phenomena may share roles of importance in dynamic stall. The unsteady pressure distribution has been shown to be of importance due to the alleviation of gradients over the airfoil upper surface.[9] It has been argued that the Karman-Sears/Theodorsen representation of unsteady-potential flow could account for part of the overshoot in lift. As developed for the linear perturbation problem these theories account for lift lag and attenuation, and it is difficult to justify their use in the stall problem. Because of the rates and amplitudes of motion involved, it should be assumed that non-linear potential flow is

involved. However, the pressure gradient present in the Karman-Sears type theory is of the correct behavior, as shown by Carta.[9]

The leading edge bubble, common to many airfoils used for helicopter rotors, may well play an important part in stall delay. A bubble-burst criterion has been developed by Crimi[10] for determining the stall condition. Other phenomenological devices have been used with some success, such as induced camber[7], and the "spinning cylinder" effect at the leading edge, as given by Ericsson and Reding.[11]

The actual process of flow breakdown at the instant of stall has been a point of some controversy in the past. The observations of McCroskey[3], and the work of Ham[5], and Scruggs[12], indicate the presence of discrete leading edge vortex rollup at stall. Others, including Crimi[10], have developed the idea of a "deadwater" region immediately following bubble-burst at stall. Serious theoretical questions concerning the time-dependent boundary-layer development come into play from this issue. In order to resolve the question of flow breakdown it is first necessary to carefully analyze the behavior of the unsteady boundary layer as the stall condition is approached. Little consideration has been given the unsteady boundary layer in dynamic-stall theories, although its importance has been recognized, or implied, by several researchers. One of the first attempts to investigate the significance of boundary-layer effects on a translating rotor was made by Hicks and Nash.[4] Their calculations showed that three-dimensionality in the boundary layer had a small but significant effect on separation. However, the more important result was that

both the two-and the three-dimensional calculations were found to be seriously pessimistic when the predicted separation boundaries were compared with test results for an actual rotor. The discrepancy was attributed chiefly to the neglect of time dependence in the boundary-layer equations. It was also a major factor leading to the perspective on the dynamic-stall problem taken in the present investigations. This perspective concentrates on the mechanism by which the boundary layer manages to remain attached during the dynamic overshoot, rather than on the mechanism by which stall finally does take place. At significant rates of pitch, the boundary layer stays attached to the airfoil -- or at least behaves as though it were still attached -- at angles of incidence substantially higher than could occur under static conditions.

The suggestion that unsteady effects in the boundary layer itself (as distinct to those in the external flow) cause, or contribute to the tenacity of the boundary layer referred to above, was confirmed by the work of Singleton et al.[13] and Nash et al.[14] Their work showed that time-dependence results in a delay in the onset of flow reversal in the boundary layer, and that this delay could be large under conditions simulating the flow over an airfoil in upward pitching motion. Now, in unsteady flow, reversal and separation are generally distinct phenomena. Reversal refers to conditions in the inner part of the boundary layer, adjacent to the airfoil surface, and its onset corresponds to the vanishing on the wall shear stress. Separation, on the other hand, refers to detachment of the outer flow from the airfoil

contour, and the breakdown of the boundary-layer equations. The work of Sears and Telionis[15] indicates that, for flows of the present type, separation would always occur later than reversal. Thus, any prediction of the delay in flow-reversal onset has to be regarded as a conservative estimate of the delay in separation onset. Correspondingly, and this is the point which is relevant to the present studies, if it can be shown that reversal is avoided over some range of incidence, due to dynamic effects, then it can safely be concluded that separation will be avoided over at least the same range of incidence. These comments refer only to the upstroke of the airfoil motion, which is the situation addressed herein; under conditions corresponding to the downstroke, separation preceeds reversal and avoidance of reversal does not imply avoidance of separation.

The work of References (13,14) examined the nature of the unsteadiness in a boundary layer developing in a prescribed external velocity distribution. The flow over an airfoil in pitching motion is, however, more general than this, insofar as the external velocity field itself depends on the pitch rate. Thus a second source of unsteady effects is presented by the departure of the external velocity distribution, at any given incidence, from its form in steady flow. Both sources of unsteadiness are considered in the present calculations, and one of the objectives of the present study was to determine their relative importance in the context of flow-reversal onset.

THEORETICAL DEVELOPMENT

A two-dimensional, time dependent flow is assumed. For all conditions preceding that of stall, the outer potential flow is assumed to be circulation preserving. The viscous flow near the airfoil surface is assumed to obey boundary layer assumptions until the local surface shear stress falls to zero and the displacement thickness diverges, indicating the approach to separation. In order to identify the separation dynamics in the simplest possible unsteady flow consistent with observed experimental cases, it is assumed that the airfoil begins a pitch motion about its quarter-chord from a steady, zero angle-of-attack initial condition, and pitches at a constant rate until the point of flow reversal on the upper surface moves to the vicinity of the leading edge.

The concept of one-way coupling is employed and, as depicted in Figure 1, assumes that during the motion of the airfoil the boundary layer remains sufficiently thin that the unsteady potential flow is unaffected by it. This is the usual assumption made in airfoil calculations. However it should be noted that its validity is improved in unsteady flows of the type considered here because the displacement thickness is generally smaller than in equivalent steady flows: this is true near the point of flow reversal and elsewhere. The potential flow develops in response to the airfoil motion in a circulation preserving manner and imposes a pressure distribution on the airfoil which is time dependent. The mathematical model appropriate to the description of such a flow is developed in the following sections. Incompressibility is assumed throughout.

The Potential Flow

Unsteady potential flow constitutes a linear problem in the sense that the governing differential equation for any potential flow is linear. However in the time dependent case, when it is necessary to determine the instantaneous tangential velocities on a moving boundary the algebraic resolution of the problem exhibits numerical difficulties similar to those encountered in the solution of a non-linear differential equation. A method due to Giesing[16] is used in the present investigation to determine the time-dependent pressure distribution, to be imposed on the boundary layer, due to an arbitrary motion of the airfoil in a two dimensional, incompressible potential flow. The airfoil used throughout this investigation is the NACA 0012 section. The surface is defined for numerical purposes by 65 control points, distributed so as to give optimum definition of the unsteady velocity profiles on the surface. The motion of the airfoil begins from zero angle of attack to a uniform stream, and pitch-up commences with a constant pitch rate $\dot{\alpha}$, resulting in an angle of attack time history as shown in Figure 1. The discontinuity in $\dot{\alpha}$ at time zero causes a slight modification in airfoil loading at low angles of attack as will be seen. The flow is assumed to be circulation preserving and vorticity is released in the wake at each time step of the computation such that the sum of circulation about the airfoil and in the wake remains constant, that is

$$\Gamma_{wake} + \int_{airfoil} \gamma(s)ds = 0 \ , \qquad (1)$$

where the sum in this case is zero since the airfoil starts from zero angle of attack. The wake vorticity is released in the neighborhood of the trailing edge at all times during the motion and the boundary layer is assumed to have no effect on the potential flow. This situation is depicted in Figure 1.

The pressure at any point in the flow, as computed from a coordinate system fixed in the airfoil, is [17]

$$p/\rho + \frac{\partial \varphi}{\partial t} + \frac{1}{2} Q^2 - \frac{1}{2} Q_r^2 = H_\infty \tag{2}$$

where $\bar{Q}$ is the velocity vector at a point as measured in the airfoil coordinate system and $\bar{Q}_r$ is the velocity vector of the airfoil frame of reference relative to inertial coordinates.

For the viscous flow near the airfoil surface the equations of motion are of the form,

$$\rho\left[\frac{D\bar{Q}}{Dt} + 2\,\bar{\omega} \times \bar{Q} + \bar{\omega} \times (\bar{\omega} \times \bar{r})\right] = -\,\text{grad}\, p + \bar{F} \tag{3}$$

where $\bar{\omega}$ is the rotation rate of the airfoil, $\bar{r}$ is the position vector in airfoil coordinates, and $\bar{F}$ is a constitutive vector for the stresses. At the outer edge of the viscous flow let the velocity be $\bar{Q}_e$, then the equations of motion are

$$\rho\left[\frac{D\bar{Q}_e}{Dt} + 2\,\bar{\omega} \times \bar{Q}_e + \bar{\omega} \times (\bar{\omega} \times \bar{r})\right] = -\,\text{grad}\, p. \tag{4}$$

The two cross-product terms in equations (3) and (4) are apparent acceleration terms due, in the present case, to the pitch rate of the airfoil coordinate system. The unsteady Bernoulli equation in non-inertial coordinates, equation (2), has terms which just balance the apparent acceleration terms in equations (3) and (4). In order to couple the boundary layer approximation of equation (3), which form will be given later, to the unsteady potential flow it is desirable to remove the non-inertial terms. This is accomplished by substituting for grad p from equation (4). Then

$$\frac{D\bar{Q}}{Dt} - \frac{\bar{F}}{\rho} = \frac{D\bar{Q}_e}{Dt} \tag{5}$$

To the boundary layer approximation the right hand side of this equation (5) becomes

$$\frac{\partial U_e}{\partial t} + U_e \frac{\partial U_e}{\partial s} ,$$

where U_e is the velocity tangent to the airfoil at position s as measured in airfoil coordinates.

The centripetal acceleration along the surface thus removed was found to be small for the cases considered in the present work, being proportional to $\dot{\alpha}^2$. However for higher pitch rates this effect may become important. It is noted that the result, equation (5), does not remove the Coriolis gradient. But this gradient is everywhere normal to the airfoil surface and thus does not enter into the boundary layer momentum equation.

Since the potential flow is unaffected by the boundary layer, it may be computed for any number of time steps at each desired pitch rate and the resulting velocity distribution may then be used as forcing function for the boundary layer computation. The computations were made for both steady flow and unsteady flow for purposes of evaluating certain boundary layer effects, as will be discussed later. In every case the potential flow computation was terminated when the angle of attack reached 25°. The pitch rate parameter $c\dot{\alpha}/U_\infty$, was varied from zero to .10. The pitch axis was taken at the 25% chord. To evaluate the numerical accuracy of the unsteady wake calculation, 10 time steps were used and then 20 steps. No practical difference in airfoil loading could be detected for the highest pitch rate used. By the method of Giesing, an incremental vortex is released in the wake at each step in time. It appears that even for the most unsteady case analyzed in the present investigation the wake roll-up is sufficiently well represented by 10 incremental vortices. This result agrees with the conclusion of Geising for the highly unsteady step-start condition.[16]

Figure 2 shows a comparison of the lift coefficient versus angle of attack resulting from the potential flow program for steady and unsteady flow. The effect of the step input of $\dot{\alpha}$ is evident at the lower angles of attack, which corresponds to short intervals of time after initiating the motion. Figure 3 and Figure 4 show the velocity and pressure distributions respectively over the upper surface of the NACA 0012 at an angle of attack of 15° for the steady and unsteady conditions. It is clear that the unsteady distributions for $c\dot{\alpha}/U_\infty = .06$, show considerable

alleviation of gradients over most of the surface. Of course these figures only depict one instant of time in comparing the steady, or quasi-steady, and the unsteady flows. The alleviation of gradient is present to a greater or lesser extent throughout the pitch-up motion. It can be expected to contribute to a delay in boundary-layer flow reversal in addition to the delay associated with unsteadiness in the boundary layer itself.

The Unsteady Boundary Layer

The original method of Patel and Nash[18] for unsteady turbulent boundary layers has been recently improved upon and used as a basis for a range of computational experiments.[13], [14], [19] The theory is presented here for incorporation in a fully unsteady-flow examination of the delay in reversal point movement on a practical airfoil.

The method is designed to calculate the time-dependent, incompressible, turbulent boundary layer on a two-dimensional airfoil section moving in a potential flow field. A curvilinear coordinate system is fitted to the airfoil surface: s denoting distance along the surface, y the distance along the local normal, and x the distance along the chordline. The radius of curvature is assumed to be everywhere large compared to the boundary layer thickness. The method is given here for two dimensional unsteady flow. A somewhat more general quasi-three-dimensional formulation may be found in Reference (19).

The velocities in the s and y directions are expressed in the form

$U + u$, $V + v$, where all components are functions of s, y, and time t. The components, $U(s,y,t)$ and $V(s,y,t)$ are defined as ensemble averages, taken over a large number of realizations of the same basic flow, or successive flows with the same time history and boundary conditions. The components u and v represent the random fluctuations about U and V, and by implication their ensemble averages are identically zero.

The conservation of mass then takes the form

$$\frac{\partial U}{\partial s} + \frac{\partial V}{\partial y} = 0 \tag{6}$$

which can be immediately integrated to give V in quadrature form,

$$V = - \int_0^y \frac{\partial U}{\partial s} \, dy \ . \tag{7}$$

Applying the boundary layer approximation to equation (5) for the momentum balance in the s-direction there results

$$\frac{\partial U}{\partial t} + U \frac{\partial U}{\partial s} + V \frac{\partial U}{\partial y} - \frac{1}{\rho} \frac{\partial \tau}{\partial y} = \frac{\partial U_e}{\partial t} + U_e \frac{\partial U_e}{\partial s} \ , \tag{8}$$

where the viscous shear stress has been neglected and the turbulent shear stress, τ , is the ensemble average,

$$\tau = - \rho \, \overline{uv} \ . \tag{9}$$

The turbulent shear stress is assumed to behave according to a rate equation which follows from those given for three dimensional flows, [20],[22] but with the convective derivative extended to include the time derivative,[18]

$$\frac{\partial(\overline{uv})}{\partial t} + U\frac{\partial(\overline{uv})}{\partial s} + V\frac{\partial(\overline{uv})}{\partial y} + 2\,a_1\,(\overline{uv})\frac{\partial U}{\partial y} \qquad (10)$$

$$+ \frac{\partial}{\partial y}(a_2\,\overline{uv}) + \frac{\overline{uv}^{3/2}}{L} = 0 \ .$$

For most of the calculations, a_1 , a_2 , and L are assumed to be the same functions as appear in the earlier steady and unsteady three-dimensional methods[19],[20]; a_2 and L are shown by the solid curves in Figure 5, and a_1 is taken to be the usual constant (= 0.15). The validity of these empirical functions has never been checked directly, for unsteady flow, because of the lack of experimental data. In order to determine the sensitivity of the results to changes of the dissipation length function (the most critical one), some calculations were done using the dashed curve in Figure 5. The flat dissipation length, over the outer part of the boundary layer, leads to a more constant distribution of turbulent kinetic energy. It was found, however, that the calculated velocity profiles and the predicted point of flow reversal were almost indistinguishable from the results corresponding to the original dissipation length. Uncertainties in the empirical functions do not, therefore, seem likely to put the present results seriously in question.

Since the turbulent boundary layer thickness varies rapidly in both

space and time, the extent of the domain of numerical integration is a variable calculated continuously as the computation proceeds. Thus a transformation

$$\begin{aligned} t &= t^* \\ s &= \xi \\ y &= h(s,t)\eta^{\beta} \end{aligned} \tag{11}$$

is introduced where β is a constant greater than unity, and h is the height of the computation. h is allowed to increase (or decrease) in sympathy with the boundary layer thickness $\delta(s,t)$, and an approximate proportionality is maintained between them. This proportionality cannot be made exact in an explicit scheme since the value of $\partial h/\partial s$ must be assigned before $\partial\delta/\partial s$ is known. h is taken to be about 1.25δ. Primary mesh points lie on curves of constant y/h, and are distributed nonuniformly over the height of the domain to produce an increased density of points near the surface. If the points are distributed such that y_i is proportional to $(i - 1)^{\beta}$, the transformation(11) will transform the domain into one of constant thickness and uniform η-step.

Having made the transformation(11) and defining matrices as follows,

$$F = \begin{bmatrix} U \\ \overline{uv} \end{bmatrix} , \qquad C = \begin{bmatrix} c_1 \\ c_2 \end{bmatrix} ,$$

$$A = \begin{bmatrix} a_{11} & a_{12} \\ a_{21} & a_{22} \end{bmatrix} , \qquad B = \begin{bmatrix} b_{11} & 0 \\ 0 & b_{22} \end{bmatrix} \tag{12}$$

the governing equations take the form

$$\frac{\partial F}{\partial t} = A \frac{\partial F}{\partial \eta} + B \frac{\partial F}{\partial s} + C \tag{13}$$

where the a_{ij}'s , b_{ij}'s , c_i's $(i,j = 1,2)$ are functions of the dependent variables. The system of equation (13) is hyperbolic, and is integrated in a three-dimensional domain (η,s,t) by means of an explicit, staggered-mesh, finite-difference scheme. A fourth-order accurate difference formula is used for the $\partial/\partial\eta$:

$$\Delta\eta \left(\frac{\partial F}{\partial \eta}\right)_i = \frac{1}{12} F_{i-2} - \frac{2}{3} F_{i-1} + \frac{2}{3} F_{i+1} - \frac{1}{12} F_{i+2} \tag{14}$$

where the subscript i denotes the value of $F(\eta = \eta_i)$,

$$\eta_i = \frac{i-1}{n-1} , \tag{15}$$

and n = total number of mesh points across the boundary layer. Equation (14) cannot be used for $i = n - 1$ and in this case, it is replaced by the third order accurate scheme:

$$\Delta\eta\left(\frac{\partial F}{\partial \eta}\right)_{n-1} = \frac{1}{6} F_{n-3} - F_{n-2} + \frac{1}{2} F_{n-1} + \frac{1}{3} F. \qquad (16)$$

Boundary conditions for the calculation consist of:

1) initial profiles of U and $\overline{uv}$ versus y for $t = 0$ and x,

2) initial profiles of U and $\overline{uv}$ versus y for $x = 0$ and all t,

3) $\frac{\partial U}{\partial y} = \frac{\partial uv}{\partial y} = \overline{uv} = 0$, at $y = 1.25\delta$

   1.25δ being the local height of the integration domain, which varies with both x and t.

4) appropriate boundary conditions at $y = 0$, which are imposed by matching the numerical solution to the Law of the Wall at $y/\delta = 0.05$.

In the method of Singleton and Nash,[19] integration of the above equations is carried out in the direction of increasing time: profiles of velocity and shear stress being calculated for all x, over successive planes t = constant. This procedure results in a stability condition restricting Δt to some value which depends on the minimum boundary-layer thickness at the particular time level. For calculations of the present type, in which the boundary-layer thickness is very small near the leading edge, the procedure would have led to excessive machine

times. Instead, the roles of time and chordwise position were reversed. The present calculations were performed with the integration advancing in the positive x-direction, profiles for all t being determined over successive planes x = constant. As before, proper consideration was given to the zones of dependence and influence associated with the convection of information in the flow. The scheme provided for either first- or second-order accuracy in the time direction; sample calculations indicated little difference in the results obtained.

The finite-difference molecule is shown in Figure (6), and the scheme is given by

$$F_c = \frac{1}{2}\left(F_A + F_B\right) + \frac{1}{8}\Delta\eta\left[\left(\frac{\partial F}{\partial \eta}\right)_A - \left(\frac{\partial F}{\partial \eta}\right)_B\right] \qquad (17)$$

$$+ \frac{1}{2}\Delta s\left[\left(\frac{\partial F}{\partial s}\right)_A + \frac{\partial F}{\partial s_B}\right]$$

This scheme has been shown by Nash[22] to be both second-order accurate and conditionally stable.

The boundary-layer calculations covered the region of non-reversal flow on the airfoil (Figure 7). No attempt was made to penetrate beyond the instantaneous point of flow reversal, at each time level, although this has been done in more recent calculations which are continuing at the time of writing. The present calculations were started at a "transition line," which is assumed to coincide with the suction peak on the airfoil, and which moves forward as the angle of incidence increases with time. In order to generate initial conditions for the turbulent boundary-layer

simple quasi-steady laminar calculations were performed for the region between the instantaneous stagnation line and the transition line as defined above. It was decided to maintain continuity of momentum thickness across the transition line if the Reynolds number based on momentum thickness, R_θ, exceeded 320 (assumed to be the minimum value for a fully-developed turbulent boundary layer). If the value of R_θ, from the laminar calculation, was less than 320, it was decided to impose a step change in momentum thickness to bring R_θ up to the prescribed minimum level. It emerged that the step change was necessary in virtually all the calculations done in this study(in fact up to a chord Reynolds number of 3×10^6). The initial velocity and shear-stress profiles were then constructed, using the momentum thickness derived in this manner, as though the boundary layer corresponded locally to steady flow over a flat plate. The procedure adopted for generating the initial profiles was clearly crude. It provided a measure of consistency throughout the calculations, and fortunately the results did not seem unduly sensitive to small changes from the assumed conditions. A more detailed treatment of the initial conditions is needed, although it involves the very complex problem of unsteady transition near a high suction peak. Both experimental and theoretical work is probably needed before reliable guidelines can be provided for calculations of the present type.

RESULTS AND COMPARISONS WITH EXPERIMENT

The primary objective of this numerical study was to assess the effects of time-dependence on the onset of flow reversal in the boundary layer. As noted earlier, these effects arise in two ways: in the potential flow about the airfoil in unsteady motion, and in the response of the boundary layer to the velocity distribution imposed by the unsteady potential flow. The present work attempts to determine both the overall effect of the time-dependence and the relative importance of each component.

For simplicity, the time history of the airfoil motion was idealized by uniform motion, at zero incidence, for $t \leq 0$, followed by a constant rate of pitch, for $t > 0$. This simple situation provides well-defined initial conditions at the time origin, and an unsteady flow defined by a single parameter thereafter. The single parameter is the rate of pitch: $\dot{\alpha}$, which can be expressed non-dimensionally as a sort of "reduced frequency" $c\dot{\alpha}/U_\infty$, where c is the airfoil chord and U_∞, the free-stream speed, although the flow is not, of course, oscillatory. Oscillatory flow was avoided both because of the higher time derivatives present and because the initial conditions would be difficult to specify at any given instant of time.

The calculation was performed in two steps: first, the potential-flow calculation, to produce the external velocity distribution (as a function of chordwise position and time), and then the boundary-layer calculation using this velocity distribution. The calculations were done on the

CDC 6600 machine. Run times varied with pitch rate, but were on the order of 1.5 minutes for each potential-flow calculation and about the same for each boundary-layer calculation.

Analytical Results and Discussion

Potential-flow velocity distributions were calculated over the upper surface of the airfoil, for incidences up to 25° and for a range of pitch rates: $c\dot{\alpha}/U_\infty$, from 0 to 0.1. This range brackets the available experimental data and also covers conditions existing on typical rotor blades. With $\dot{\alpha} \to 0$, the results correspond to steady potential flow past the airfoil at each value of $\dot{\alpha}$ considered.

Interfacing between the potential-flow calculation and the boundary-layer calculation consisted of a set of velocity distributions, $U_e(x,\alpha)$, together with the appropriate value of $c\dot{\alpha}/U_\infty$. It was possible, however, to do a steady boundary-layer calculation ($\dot{\alpha} \to 0$) using the external velocity distributions corresponding to unsteady potential flow ($\dot{\alpha} > 0$). Alternatively, an unsteady boundary-layer calculation could be performed using the set of external velocity distributions correspoining to steady potential flow. Thus four combinations of conditions existed:

1) steady potential flow, steady boundary layer
2) steady potential flow, unsteady boundary layer
3) unsteady potential flow, steady boundary layer
4) unsteady potential flow, unsteady boundary layer.

Combination (1) represents flow at a vanishingly small rate of pitch

($\dot{\alpha} \to 0$); (4) represents the fully unsteady flow at some given $c\dot{\alpha}/U_\infty$. Combinations (2) and (3) represent approximations to the true state of affairs, in which time-dependence is assumed to be present in either the potential flow or the boundary layer, but not both, the objective being to determine the relative importance of each effect.

Calculations, covering these four combinations, were performed for some 12 values of $c\dot{\alpha}/U_\infty$, from 0 to 0.1, and typical sets of results are shown in Figures 8 through 13. Each figure shows the movement of the flow-reversal point with angle of attack (or with time, since the two are proportional to one another). The reversal point is the point where the wall shear stress first reaches zero. The behavior is qualitatively the same in each case, and can be divided into three phases. At low angles of incidence, below about 8°, there is little movement of the reversal point away from the trailing edge. Then, over some fairly short range of incidence the reversal point moves rapidly forward, and finally at high angles of incidence the reversal point remains close to the leading edge, with little further movement. It has to be recognized, of course, that if flow reversal occurs substantially ahead of the trailing edge -- and is accompanied by gross boundary-layer thickening or separation -- then the outer potential flow will be distorted and the external velocity distribution assumed in the boundary-layer calculation will not be the correct one. Be that as it may, the results are probably realistic up to incidences corresponding to some point in the region of rapid forward movement of reversal.

At each value of $c\alpha/U_\infty$, in Figures 8 through 13, the curve for fully unsteady flow (combination (4)) lies to the right of the one for fully steady flow (combination (1)). Thus the effect of time-dependence is to delay the onset of significant flow reversal to higher angles of incidence. The curves corresponding to combinations (2), (3) lie between those for fully steady flow and fully unsteady flow, indicating that the two components of the time-dependence each serve to delay flow reversal, compared with the steady case. The incremental effects are of roughly the same magnitude, and hence it may be concluded that the components of unsteadiness in the potential flow and in the boundary layer, are both important. The two increments are not precisely additive, because of non-linearities in the flow, and it will be noted that the significance of the nonlinearity increases with $\dot{\alpha}$.

As $\dot{\alpha}$ increases, the extent of the delay in flow reversal becomes greater, and the subsequent forward movement of the reversal point becomes progressively more rapid. At the highest values of $\dot{\alpha}$ considered, there may be a discontinuous movement of reversal point, but the time steps were too coarse to judge definitively. Analysis of the behavior of the two increments of unsteadiness indicates that the increase of the rate of forward movement of the reversal point stems chiefly from the effect of time-dependence in the boundary layer.

Except possibly at the highest values of $c\dot{\alpha}/U_\infty$ considered (see above), the forward movement of the point of flow reversal is progressive, and there is a consequent degree of arbitrariness in any measure of the onset of "significant reversal". A reasonably objective criterion of

significant flow reversal would seem to be the movement of the reversal point past some particular chordwise station lying in the steep part of the curves in Figures 8 through 13. 50% chord has been selected as an appropriate station for this purpose.

Use of a criterion of this nature permits discussion, in quantitative terms, of the delay in flow-reversal onset, with increasing pitch rate, and Figure 14 presents the data plotted versus $c\dot{\alpha}/U_\infty$. It is evident that for small values of $c\dot{\alpha}/U_\infty$ the incidence, at which significant reversal occurs, increases linearly with $c\dot{\alpha}/U_\infty$. For large values, however, nonlinearities set in and the delay in flow reversal appears to flatten out to a maximum corresponding to an increment of about 8° of incidence. The two components of the effect of time-dependence exhibit qualitatively similar behavior, as is shown by the dashed and the chain-dotted curves in Figure 14. The sum of these is seen to be a rough approximation to the results for fully unsteady flow.

In addition to examining the movement of the flow-reversal point with incidence, it is instructive to observe development of the boundary layer during the approach to incipient reversal. Figure 15 shows the chordwise variation of wall shear stress at the instant of time when the airfoil incidence equals 17.5°. These results illustrate the delay in flow reversal rather dramatically: in steady flow ($\dot{\alpha} = 0$), reversal occurs at about 0.2 chord, while in fully unsteady flow ($c\dot{\alpha}/U_\infty = 0.06$, here) it does not occur until 0.94 chord. The assumption of partially unsteady flow (either in the potential flow or in the boundary layer, but not in both) yields intermediate positions of reversal. Figure 16

shows the corresponding results for displacement thickness. At the position of steady-flow reversal (in this case, steady separation) the displacement thickness exhibits singular behavior, δ^* increasing rapidly to infinity as the wall shear stress approaches zero. In unsteady flow, however, the displacement thickness is everywhere smaller than in steady flow. As the point of unsteady flow reversal is approached the displacement thickness increases rapidly, but not so rapidly as occurred in the steady flow. A fairly rapid increase is to be expected because $\partial U_e/\partial t$ is relatively small over the rear of the airfoil (cf. the results for Flow D, in Reference 14).

Figure 17 contrasts the approach to unsteady flow reversal in space (the upper figure) and in time (the lower figure); local incidence is used here as the measure of time. The actual history of a fluid particle moving over the airfoil will be somewhere between these two extremes, depending on the value of $c\dot{\alpha}/U_\infty$ (in this case 0.06) and on its position in the boundary layer. The spacial variation of the boundary-layer parameters is initially different from their temporal variation, but the differences become less as the reversal point is approached. Indeed, representative velocity profiles (Figure 18) show essentially the same pattern, during the last stages of approach to reversal, whether the observer is fixed in space or in time.

Comparison with Experimental Results

A direct validation of the computed results, presented herein, cannot be made because of the lack of relevant experimental data. There are virtually no data available from which the movement of the flow-reversal point could be deduced -- or, indeed from which any useful boundary-layer information could be deduced. The sets of measurements discussed below provide unsteady force and moment data and, to some extent, unsteady pressure data. The comparisons between theory and experiment thus have to be properly interpreted. Comparisons are made between the calculated onset of significant flow reversal (as defined in the previous section) and the occurrence of some event identified in terms of the force, moment, or pressure measurements. The event selected is not always the same in each experiment, as will be noted later, and consequently there may be difficulty in relating one set of measurements with another. Moreover, it has yet to be established that any of the events selected is associated with the flow reversal. The intention, in making these comparisons, needs to be clarified, and it is two-fold. First, it is of considerable interest to see whether the effects of time-dependence can explain the well-behaved development of the turbulent boundary layer during the dynamic overshoot. From experiment it is known that the boundary layer remains attached, or appears to remain attached, at angles of incidence substantially higher than the static-stall angle, enabling the circulation to continue increasing. If it is found that the predicted delay in flow reversal is much <u>smaller</u> than the observed delay in stall, at a given pitch rate, then some other explanation must be found for the <u>failure</u> of the airfoil to stall. Second, it is of interest to see

whether the predicted delay of reversal and the observed delay of stall are of comparable magnitude. If they are, then the tentative conclusion may be drawn that unsteady boundary-layer calculations, of the type performed here, have some relevance to the dynamic-stall problem, and further studies can search for a possible causative link between the movement of the rear point of flow reversal and the onset of dynamic stall.

Experiments conducted by Garelick[23] approximated a ramp-type increase in angle of attack from steady initial conditions. In some instances the α-trace of reference (23) did not maintain a linear increase due to aerodynamic and inertia loading in the test apparatus. The criterion used in evaluating that data to determine stall onset was to determine the angle at which the pressure at 10% chord (of a NACA 0012 airfoil) stopped increasing. Although there is clearly a relation between the angle established by this criterion and the angle established in the present analysis for flow reversal at 50% chord, they are not necessarily equal. This is especially the case at the lower pitch rates where, as was seen from the analytical results, the rate of forward movement of the flow reversal point is slowed relative to the step-like motion at high pitch rate. With the potential flow and wake flow given time to respond, large adjustments in the pressure distributions may occur, with leading vortex formation and bubble breakdown phenomena obscuring possible comparison.

Results for an oscillating airfoil with both a sinusoidal and a skewed wave-form are given by Carta et al.[6] Again these data measure

primarily lift and moment trajectories in the α-plane. Oscillatory data is far from ideal in evaluating separation dynamics because of history effects, fixed oscillatory amplitude (i.e., in successive cycles) and, perhaps most important, because the pitch rate varies continuously throughout the motion of the airfoil. Consequently for purposes of comparison with the present theory, oscillatory experimental data was chosen with the largest possible amplitude of motions, or the criterion was used that stall occur well before reaching peak oscillatory amplitude. When the stall occurs near the maximum angle, the pitch rate is changing rapidly thus the data are not suitable for comparison with constant pitch rate results. The angle of stall is determined from the data of reference (6) as the angle corresponding to sudden change in lift curve slope on the up-stroke motion.

The Reynolds number of the Garelick data is approximately 350,000, which gives a static stall angle of 10° (experimental) for the NACA 0012 airfoil. Figure 19 shows the predicted angle for flow reversal at 50% chord versus $c\dot{\alpha}/U$, reproduced from Figure 14, and the experimental data of Garelick and Carta, references (23) and (6) are shown for comparison. The reference (6) data is for a Reynolds number of 1×10^6, the same as that used for the theoretical results. Two additional experimental points are included, taken as given in reduced form by Ericsson and Reding, but originating in the experimental work of Steiner[24] for oscillating airfoils. These results were included to give some comparison at intermediate pitch rates, though the data are not very suited for comparison with the present theory.

Figure 19 shows that as the pitch rate parameter $c\dot{\alpha}/U$ increases, the comparison between experiment and theory improves, regardless of whether the experimental data result from approximately constant pitch rate, skewed-oscillatory, or sinusoidal test conditions. This behavior tends to confirm the observation from the calculated results that the flow reversal point moves forward more rapidly with increasing pitch rate. Thus at high pitch rate the stall is sudden and there is no observable distinction between events in the process. It is noted that the Garelick data, at a much lower Reynolds number, rise rapidly at low pitch rates then slowly approach the theoretical curve for a Reynolds number three times as large. These comparisons indicate that stall delay becomes insensitive to Reynolds number as unsteadiness increases. As a check on this observation, a short series of computations was made at Reynolds numbers of $.35 \times 10^6$ and 3×10^6, using the present theory, with no other changes being made. The results are shown in Figure 19 as the dashed curves. The calculations were made only for the full unsteady condition, that is, unsteady boundary layer and unsteady potential flow. This computation clearly confirms the observation that Reynolds number is of decreasing importance with increasing pitch rate. The theory predicts a behavior similar to the experimental values of Garelick, but with somewhat lower values of overshoot. A much more rapid increase in delay is apparent for the low pitch rates, with the curve slowly approaching that for Reynolds number one million at higher pitch rates.

CONCLUSIONS AND RECOMMENDATIONS

Conclusions

Calculations have been performed of the movement of the point of rear flow reversal on an airfoil in uniform pitching motion. The calculations were done in two stages. First, the unsteady potential flow was calculated, yielding the velocity distribution over the airfoil as a function of chordwise station and time. Then, the unsteady turbulent boundary layer was calculated using the predetermined external velocity distribution. Fully unsteady calculations, as so defined, were performed for a range of pitch rates bracketing conditions on a helicopter rotor in typical operations. In addition to these fully unsteady calculations, calculations were also performed in which either the potential flow, or the boundary layer, was considered to be quasi-steady. The objective, here, was to determine the relative importance of time-dependence in the outer flow and in the boundary-layer, from the standpoint of their effects on flow reversal.

The results indicate that a substantial delay in the onset of significant flow reversal, due to unsteadiness, occurs even at moderate rates of pitch. For high rates of pitch, the delay appears to reach a maximum corresponding to about 8° of incidence. Thus, under dynamic conditions, the turbulent boundary layer can withstand the imposed retardation, without suffering reversal, at angles of incidence up to 8° higher than would be possible under static conditions. It is known that, for flows of this type, boundary-layer separation -- in the sense of detachment of the external stream from the airfoil contour -- occurs later

than reversal. Hence, it may be concluded that the delay of separation onset is equivalent to at least 8° of incidence, at the highest rates of pitch considered here, and may even be greater.

It was found that unsteadiness in the potential flow and unsteadiness in the boundary layer both contribute, in a positive manner, to the delay of flow-reversal onset discussed above. The two effects are roughly equal in magnitude although, because of the inherent non-linearities, the two effects are not precisely additive.

The results of the present calculations shed some light on the dynamic stall problem. No suggestion is being made here that dynamic stall occurs simply as the result of the forward movement of the point of rear flow reversal. The development of the leading-edge bubble, which has not been considered in this work, no doubt plays a major role in the abrupt loss of circulation which takes place near $C_{L_{max}}$. What has been shown is that the effects of time-dependence permit the turbulent boundary layer to remain in a non-reversed (and non-separated) condition during the so-called dynamic overshoot. Had it been demonstrated that reversal, in the turbulent boundary layer, could not be avoided at these angles of incidence and pitch rates, then some other hypothesis would have been needed to explain how the lift coefficient continues to rise, beyond the point of static stall. This hypothesis would have been required in addition to an adequate description of the mechanism of dynamic stall itself; such a description has not yet been advanced.

The possibility exists, of course, that the forward movement of the rear reversal point contributes, in some manner, to the collapse of the circulation around the airfoil. The tentative suggestion, that this movement of the reversal point triggers the events which actually cause the collapse of the circulation, receives considerable support from the comparisons between theory and experiment presented herein. It is shown that there is a surprising degree of correlation between calculations of the onset of significant flow-reversal, and measurements of the onset of dynamic stall. Further work will address the question of whether the correlation is fortuitous, or whether some causative link does indeed exist between rear flow reversal and dynamic stall.

Recommendations

The present work has drawn attention to the urgency of investigating a number of related topics in order to fully exploit, apply, and extend the technology developed herein.

1. Attention should be given to the question of initial conditions for the turbulent boundary layer. As noted in the body of the Report, a full treatment would involve the study of unsteady transition near a high suction peak, possibly associated with a separation bubble (or more precisely a bubble of reversed flow); this is a formidable problem. A useful, but more limited, approach would be to perform a sensitivity analysis to determine the precise effect of the uncertainty in initial conditions: with regard to the thickness and profile of the turbulent boundary layer, and also to the location of transition. Herein,

transition was assumed to occur at the suction peak, but it may occur shortly thereafter. It would be helpful to know, in detail, what effect such changes would have on the predicted onset of flow reversal.

2. The question of initial conditions is tied closely to that of Reynolds-number sensitivity. Only a cursory examination of Reynolds number effects was made in the present work, and a more extensive study is called for to properly exploit the capability provided by this work.

3. A study is needed to determine the effect on flow-reversal onset of changing the incidence time history of the airfoil. In particular, there is an urgent need to compare the present results with calculations for a sinusoidal incidence pattern, so, as to approach more closely conditions on a helicopter in flight.

4. Calculations need to be performed for different airfoil sections, particularly to explore the flow-reversal behavior of some of the advanced airfoils being considered for rotor applications.

5. The present results indicated the possibility of discontinuous forward movement of the flow reversal point at high (but still realistic) pitch rates. Behavior of this type could represent an undesirable characteristic with possible load and safety implications. The significance of discontinuous movement should be considered, and the possibility of avoiding such behavior, by careful design of the airfoil pressure distribution, should be investigated. This investigation could profitably be coupled with that in 4, above.

6. The present study did not include the effects of strong interaction between the boundary layer and the potential flow. Accordingly, the validity of the results is in question once reversal moves substantially forward from the trailing edge. There is an urgent need to remove this limitation, and develop methods for including the effects of distortion of the external flow by the boundary-layer displacement thickness. Some attempts have already been made to do this, but they have largely been unsuccessful. One of the main weaknesses of these attempts has been the lack of adequate models of the boundary layer downstream of the point of flow reversal. Work currently being conducted for USAAMRDL, Ames Directorate under Contract NAS2-7724, has provided the capability of extending the boundary-layer calculation through the crucial region between reversal and flow separation. This new capability provides an essential tool for inclusion in any method of treating the strong interaction problem on a physically realistic basis.

REFERENCES

1. J. Liiva, F. J. Davenport, L. Gray and I. C. Walton, "Two-Dimensional Tests of Airfoils Oscillating Near Stall," Vol. 1 USAAVLAB Technical Rep. No. 68-13A, April 1968.

2. (Anon)., Specialists Meeting on Helicopter Rotor Loads Prediction Methods; 36th Meeting of the Structures and Materials Panel, A.G.A.R.D., Milan, Italy, March 1973.

3. W. J. McCroskey, "Dynamic Stall of Airfoils and Helicopter Rotors," in A.G.A.R.D. Rep. No. 595.

4. J. G. Hicks and J. F. Nash, "The Calculation of Three-Dimensional Turbulent Boundary Layers on Helicopter Rotors," NASA CR-1845, May 1971.

5. N. D. Ham, "Aerodynamic Loading on a Helicopter Blade During Pitching Motion in the Presence of Stall," Sc.D. Thesis, Massachusetts Inst. of Technology, January 1968.

6. F. O. Carta, G. L. Commerford, R. G. Carlson and R. H. Blackwell, "Investigation of Airfoil Dynamic Stall and Its Influence on Helicopter Control Loads," U.S.A.A.M.R.D.L. Technical Rep. No. 72-51, September 1972.

7. L. E. Ericsson and J. P. Reding, "Unsteady Airfoil Stall," NASA CR-66787, July 1969.

8. P. Crimi and B. L. Reeves, "A Method for Analyzing Dynamic Stall," A.I.A.A. 10th Aerospace Sciences Meeting, Paper No. 72-37, January 1972.

9. F. O. Carta, "Effect of Unsteady Pressure Gradient Reduction on Dynamic Stall Delay," Engineering Note, J. Aircraft, October 1971.

10. P. Crimi, "Analysis of Stall Flutter of a Helicopter Rotor Blade," A.I.A.A./A.S.M.E./S.A.E. 14th Annual Structures, Structural Dynamics, and Materials Conference, Paper No. 73-403, March 1973.

11. L. E. Ericsson and J. P. Reding, "Unsteady Airfoil Stall and Stall Flutter," Final Technical Rep., Contract NAS1-9987, June 1971.

12. R. M. Scruggs, "An Investigation of Near Wake in Airfoil Dynamic Stall," G.I.T.A.E.R. Rep. No. 71-1, March 1971, Georgia Institute of Technology (also published as Ph.D. Thesis).

13. R. E. Singleton, J. F. Nash, L. W. Carr and V. C. Patel, "Unsteady Turbulent Boundary-Layer Analysis," Final Report, Contract NAS2-6466, 1972; NASA TM X-62,242, February 1973.

14. J. F. Nash, L. W. Carr and R. E. Singleton, "Unsteady Turbulent Boundary Layers in Two-Dimensional, Incompressible Flow," A.I.A.A. 6th Fluid & Plasma Dynamics Conf., Paper No. 73-650, July 1973.

15. Sears, W. R. and Telionis, D. P., "Unsteady Boundary-Layer Separation," Recent Research on Unsteady Boundary Layers (Proc. I.U.T.A.M. Symposium, Quebec 1971), E.A. Eichelbrenner, ed., Presses de L'universite Laval, Quebec 1972.

16. J. P. Giesing, "Non-Linear Two-Dimensional Unsteady Potential Flow with Lift," J. Aircraft 5, No. 2, p. 135, 1968.

17. Sir Horace Lamb, "Hydrodynamics," Cambridge University Press, 6th Ed., 1932.

18. V. C. Patel and J. F. Nash, "Some Solutions of the Unsteady Turbulent Boundary Layer Equations," Recent Research on Unsteady Boundary Layers (Proc. I.U.T.A.M. Symposium, Quebec 1971), E.A. Eichelbrenner, ed., Presses de L'universite Laval, Quebec 1972.

19. R. E. Singleton and J. F. Nash, "A Method for Calculating Unsteady Turbulent Boundary Layers in Two- and Three-Dimensional Flows," Proc. AIAA Computational Fluid Dynamics Conference, July 1973.

20. J. F. Nash and V. C. Patel, "A Generalized Method for the Calculation of Three-Dimensional Turbulent Boundary Layers," Fluid Dynamics of Unsteady, Three-Dimensional and Separated Flows, Proceedings of Project SQUID Workshop, Georgia Institute of Technology, June 1971.

21. J. F. Nash and V. C. Patel, "Three-Dimensional Turbulent Boundary Layers," SBC Technical Books, 1972.

22. J. F. Nash, "An Explicit Scheme for the Calibration of Three-Dimensional Turbulent Boundary Layers," J. Basic Eng. 94D, p. 131, March 1972.

23. Garelick, M. S., "Non-Steady Airloads on Dynamically Stalling Two-Dimensionally Wings," Thesis, Massachusetts Institute of Technology, June 1967.

24. Steiner, R. W., "Experimental Study of the Unsteady Flow Characteristics of Stalled Airfoils," Air Force Institute of Technology, Report GAE 56-15, August 1956.

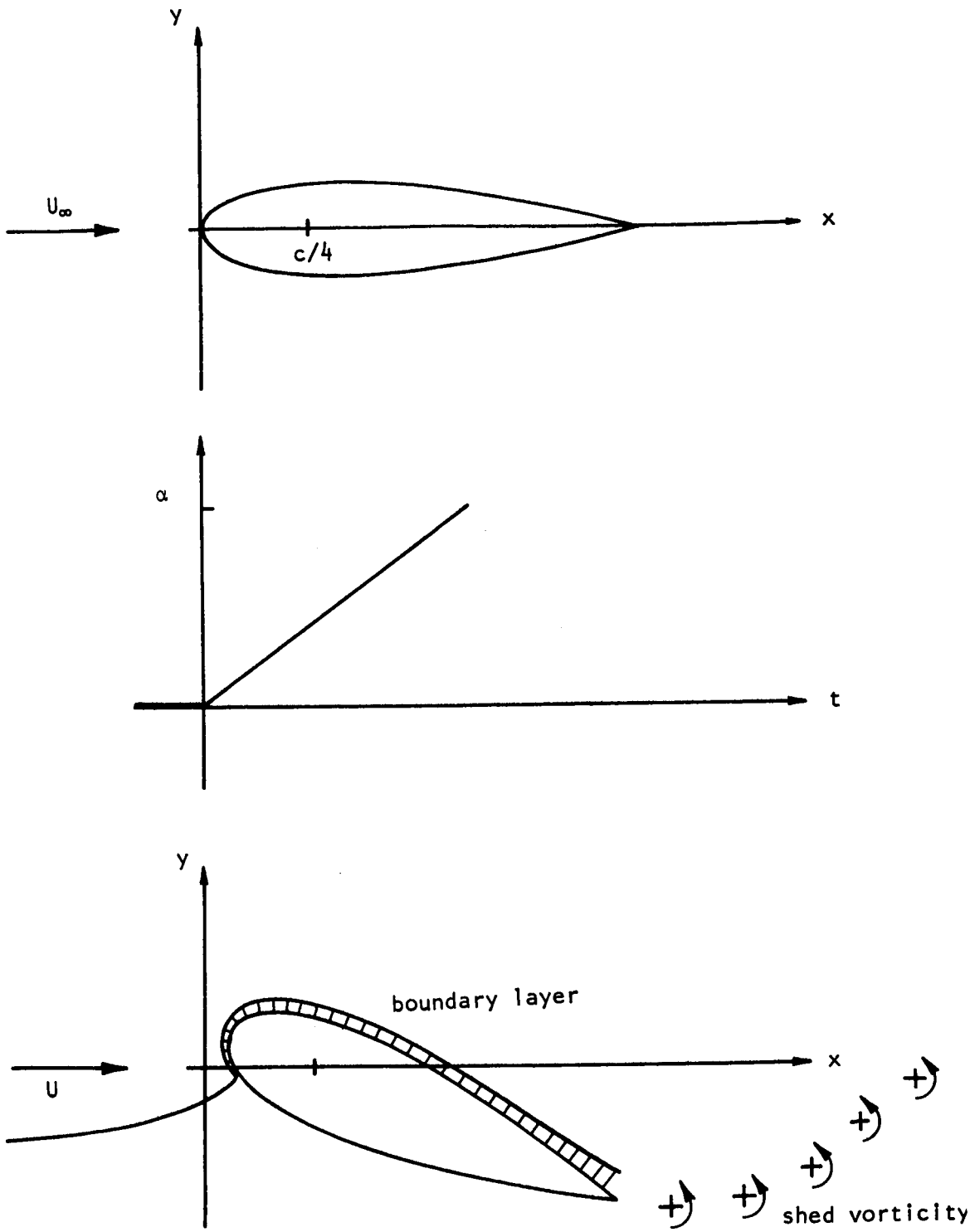

Figure 1. Schematic of the Computation Procedure

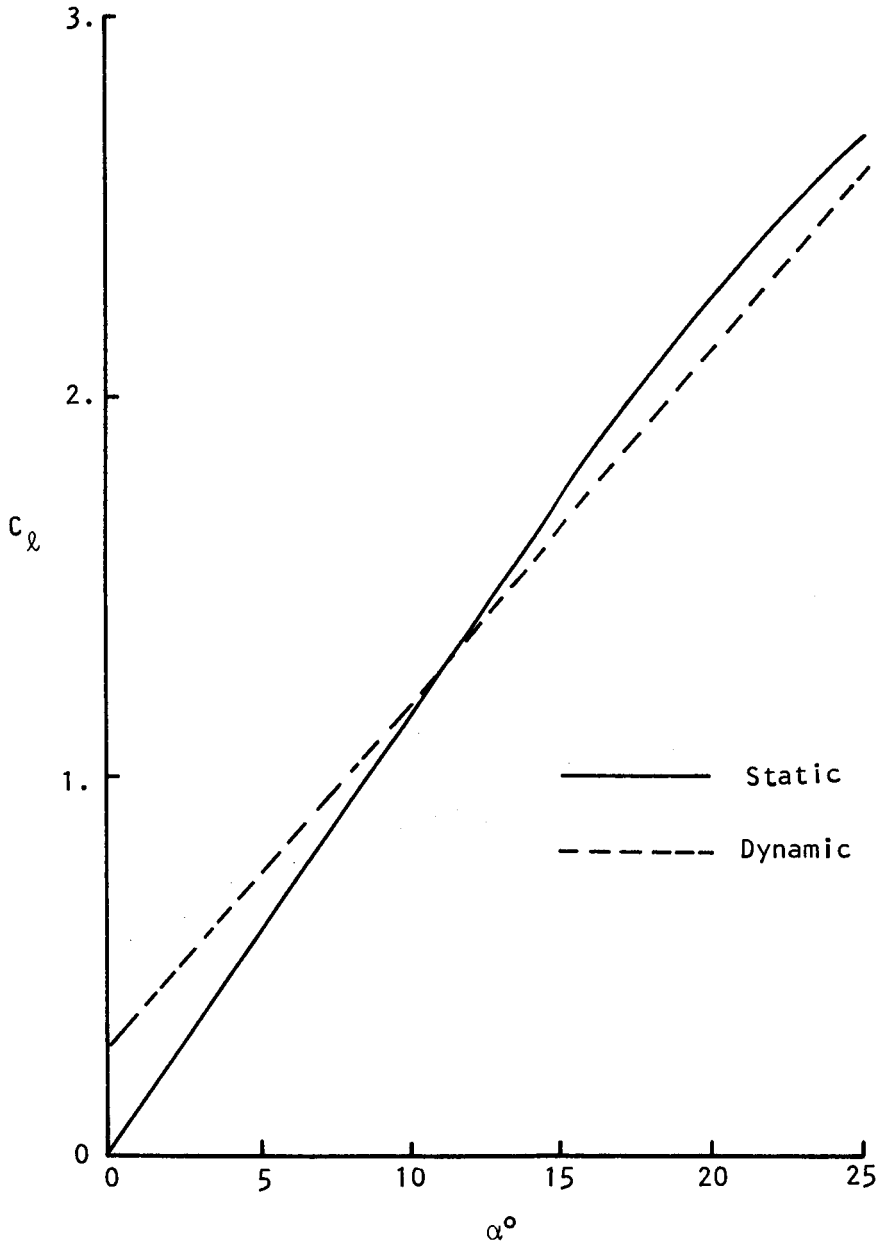

Figure 2. Unsteady Effect on C_ℓ Due to Ramp $\dot{\alpha}$

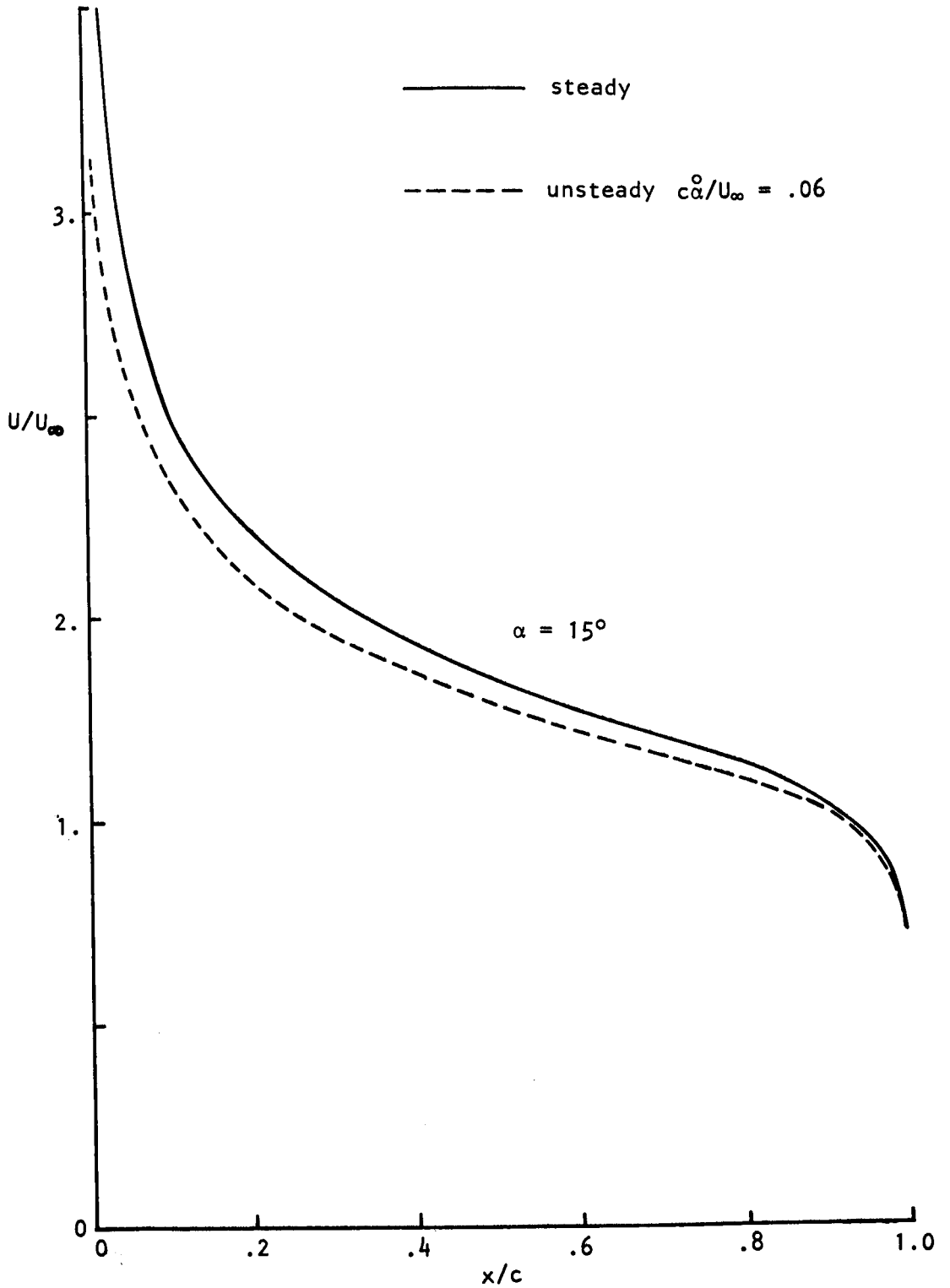

Figure 3. Pitch Rate Effect on Upper Surface Potential Flow Velocity Distribution

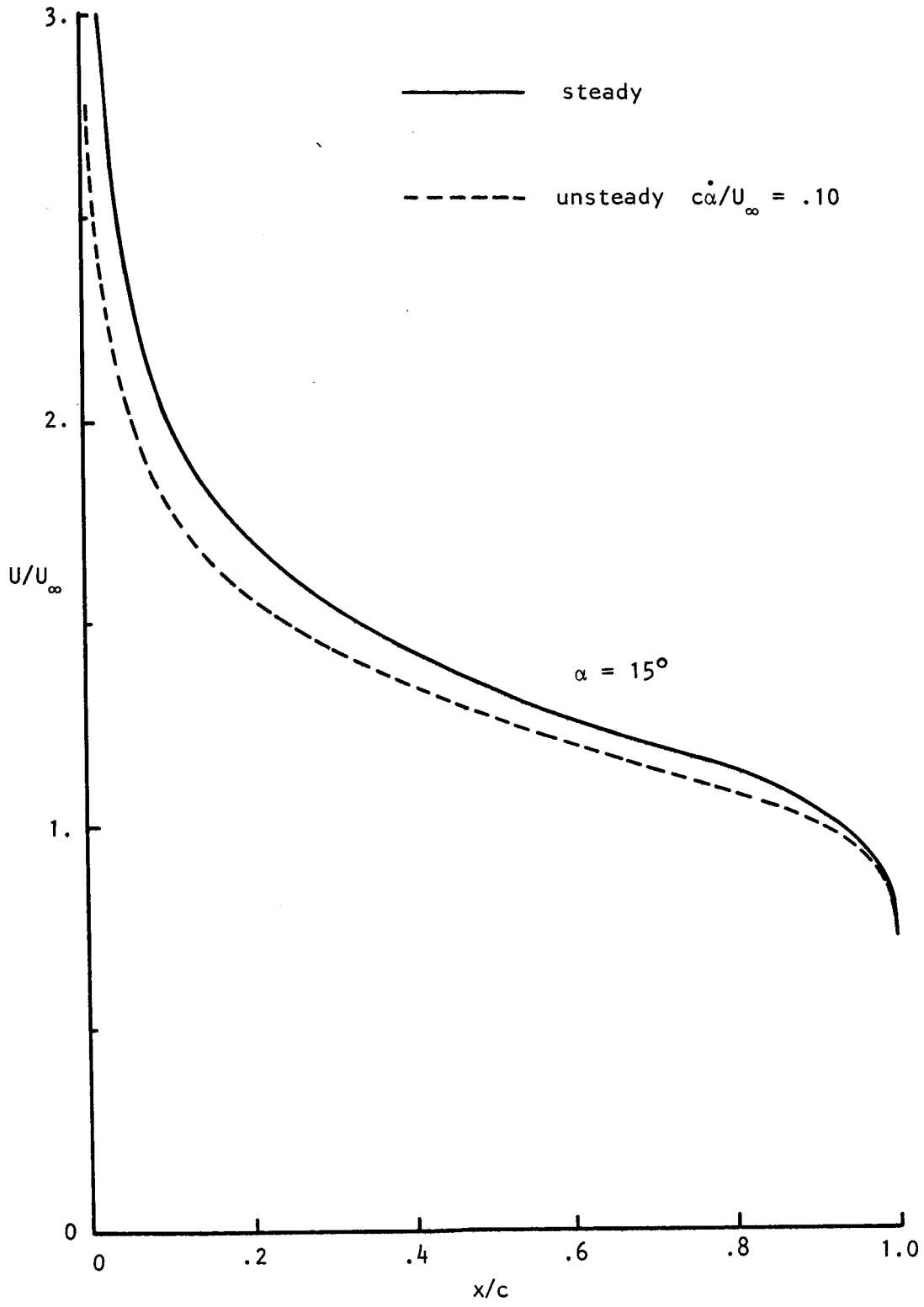

Figure 3(b). Pitch Rate Effect on Upper Surface Potential Flow Velocity Distribution

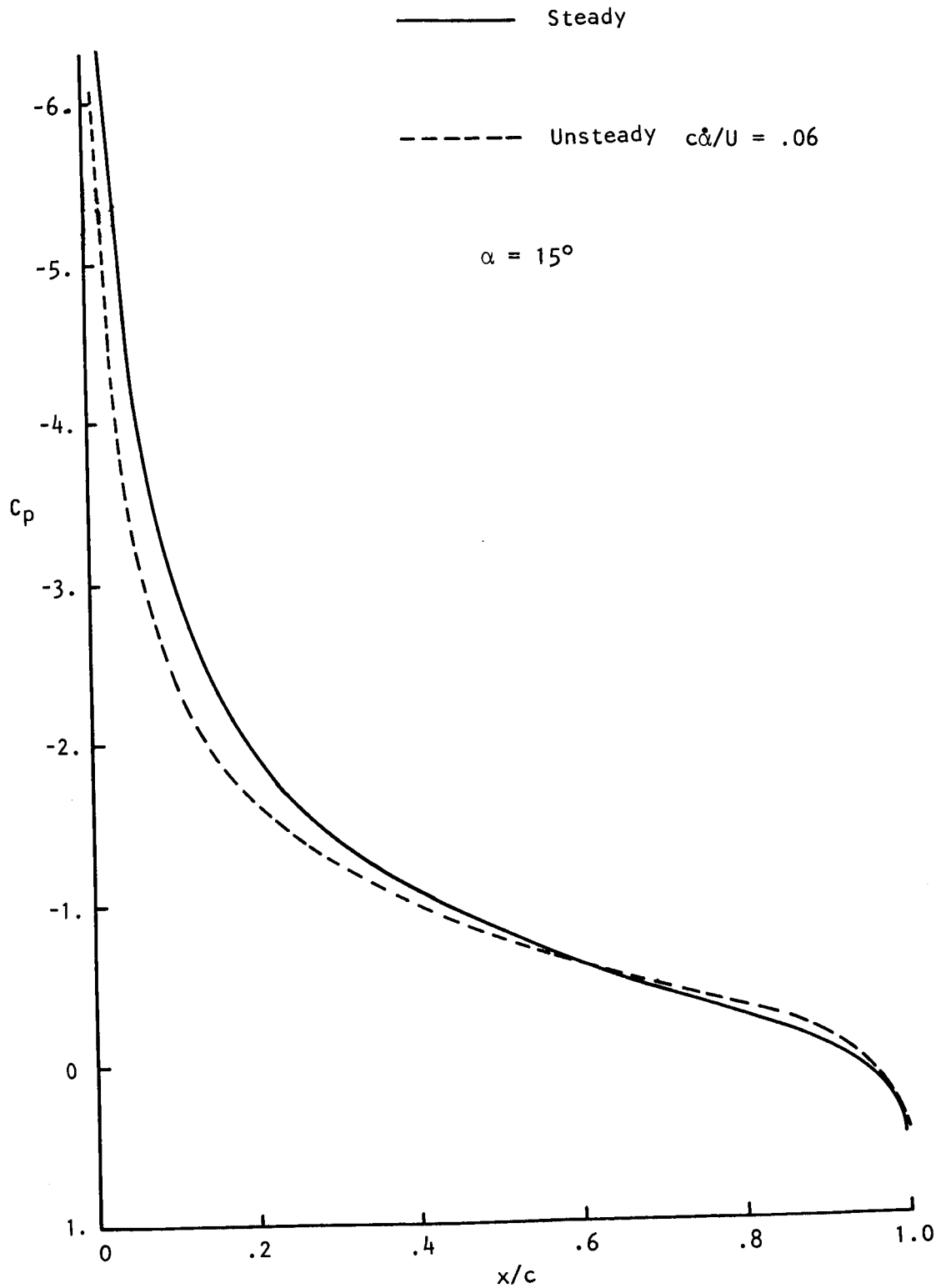

Figure 4. Pitch Rate Effect on Upper Surface Potential Flow Pressure Distribution

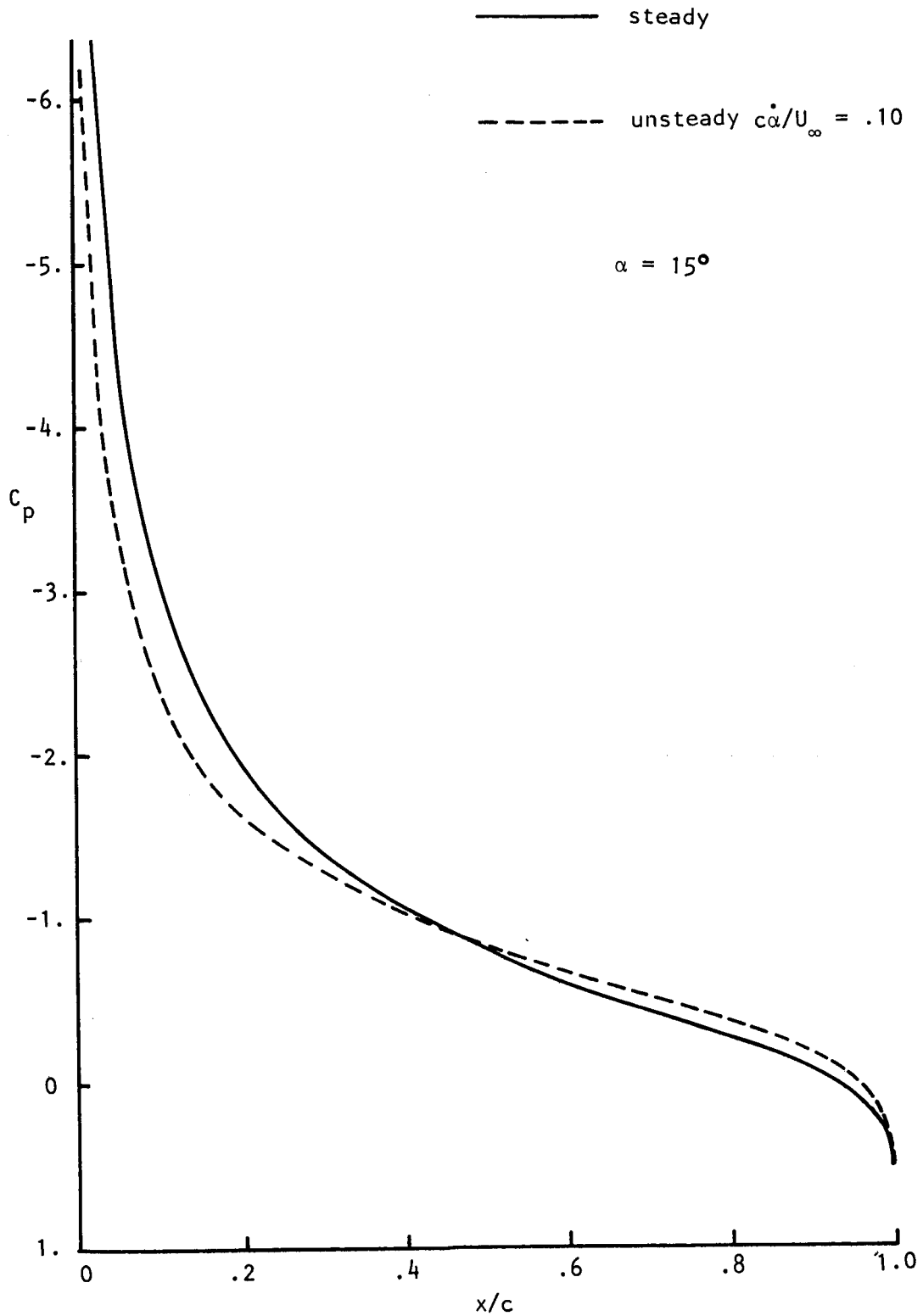

Figure 4(b). Pitch Rate Effect on Upper Surface Potential Flow Pressure Distribution

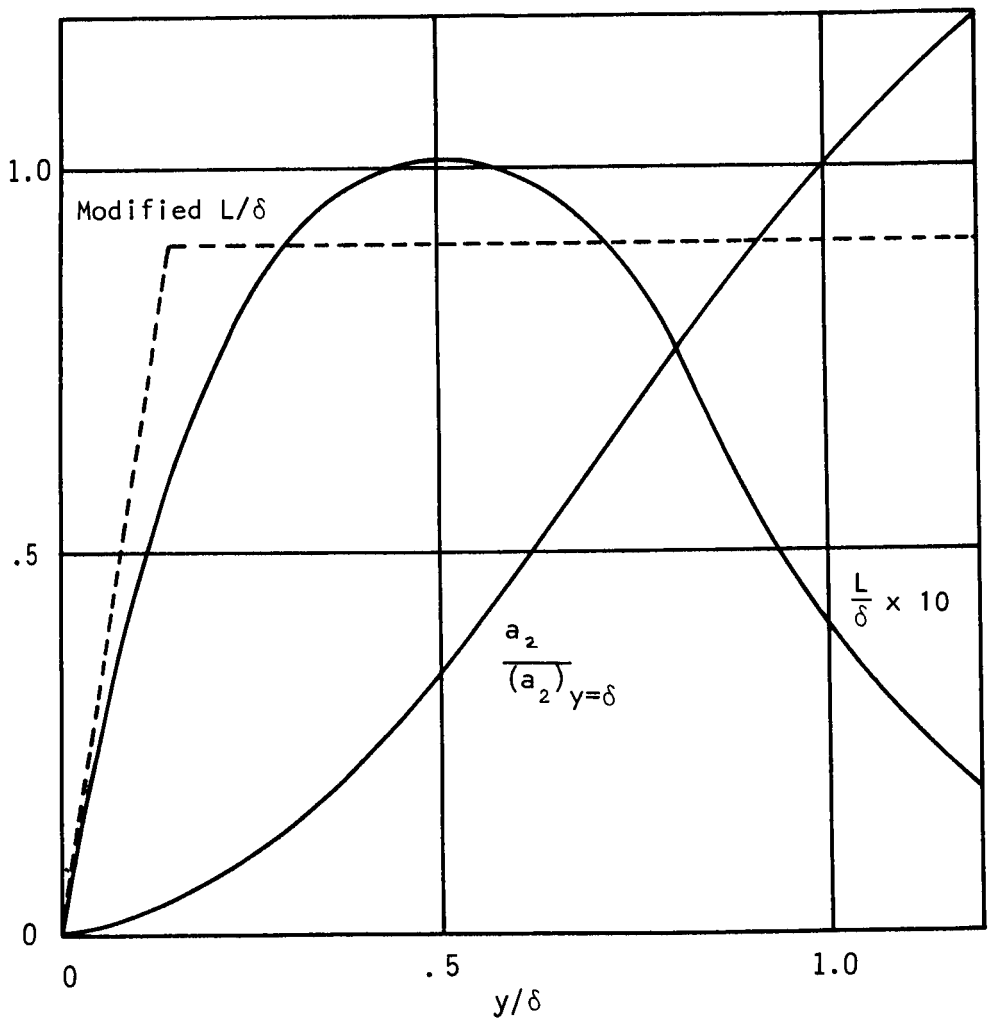

Figure 5. Empirical Turbulence Functions

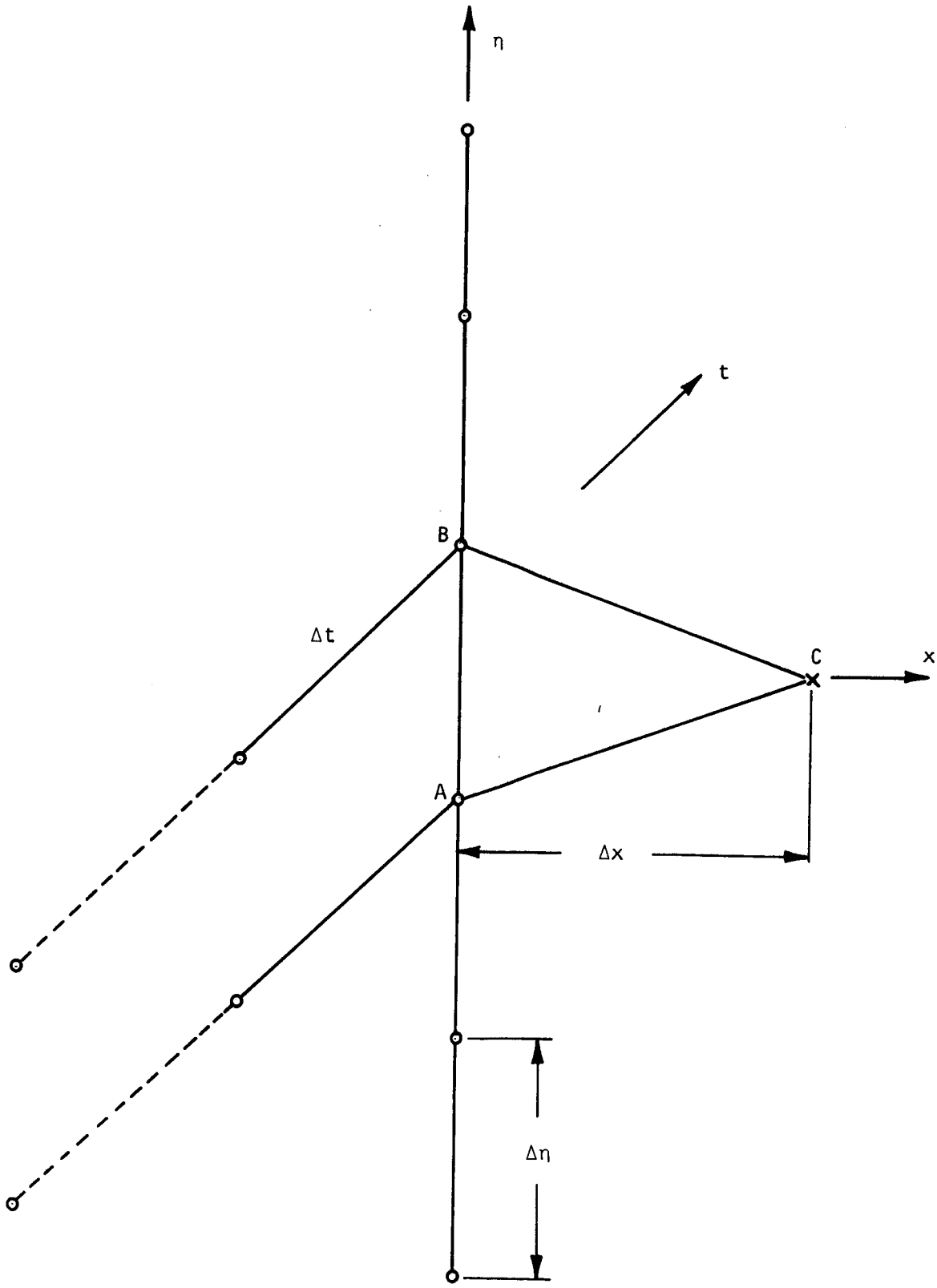

Figure 6. The Numerical Integration Molecule

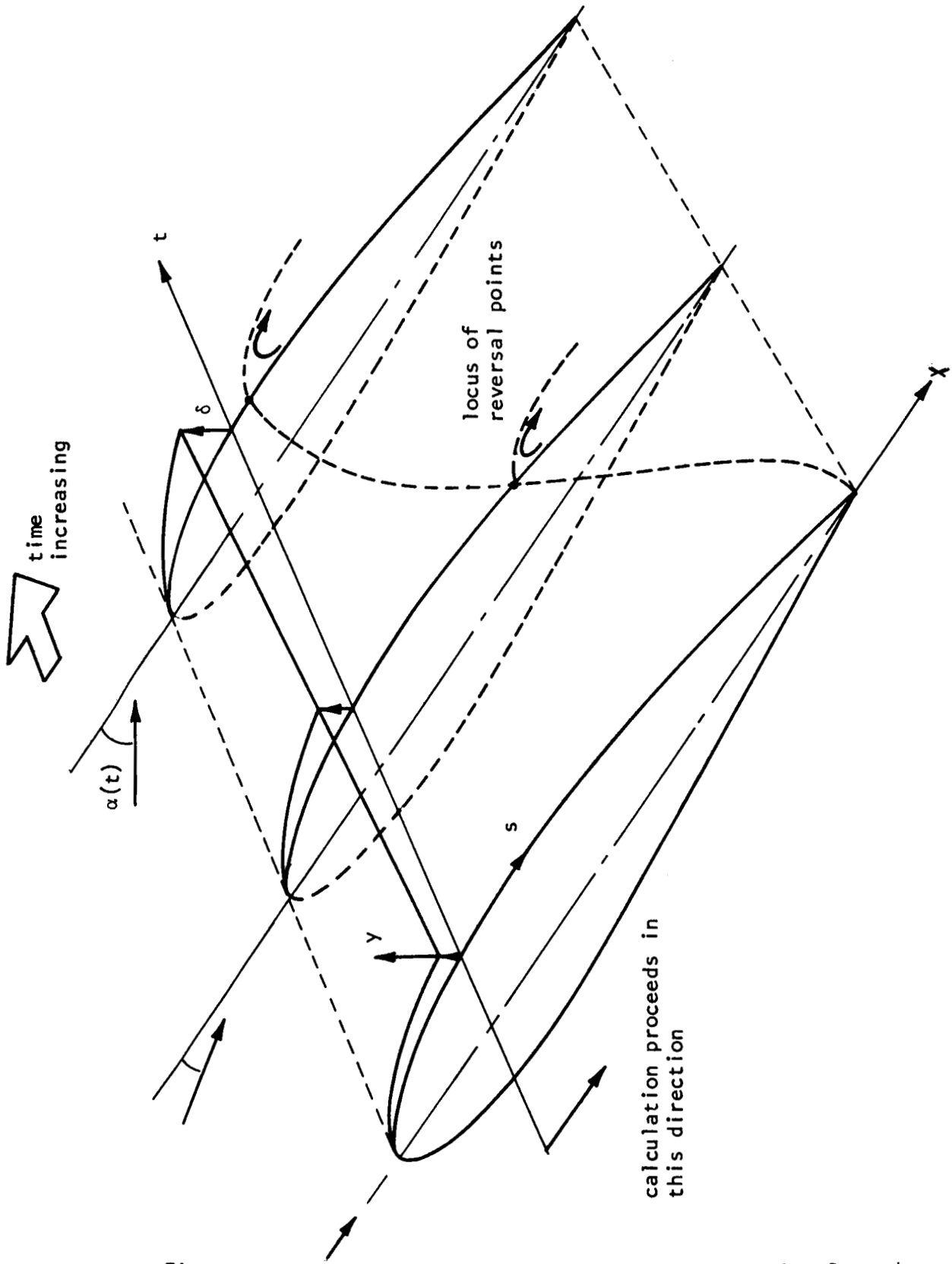

Figure 7. Schematic of the Boundary Layer Computation Procedure

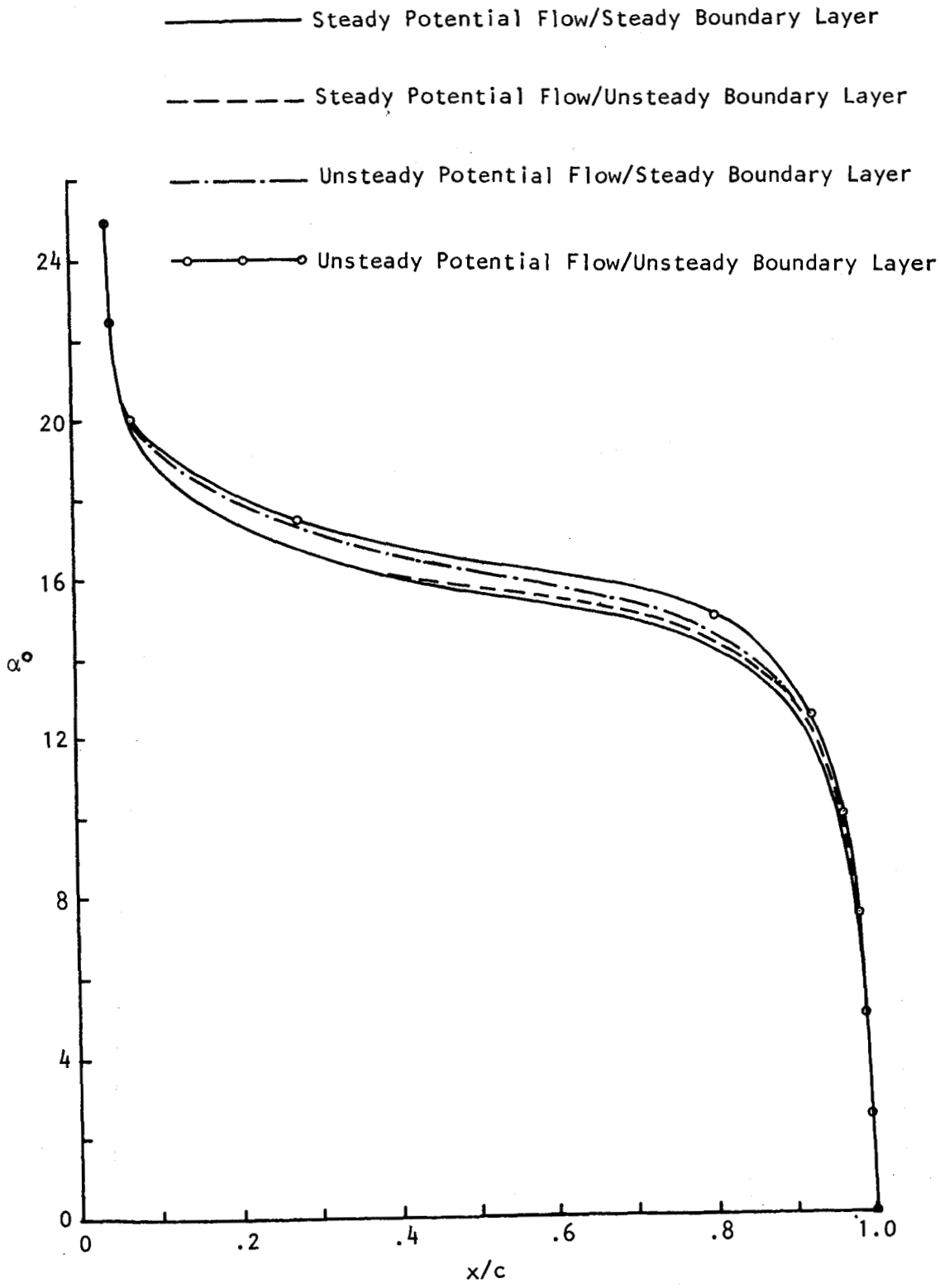

Figure 8. Forward Movement of Flow Reversal Point with Increasing Incidence, $c\dot{\alpha}/U_\infty = .005$

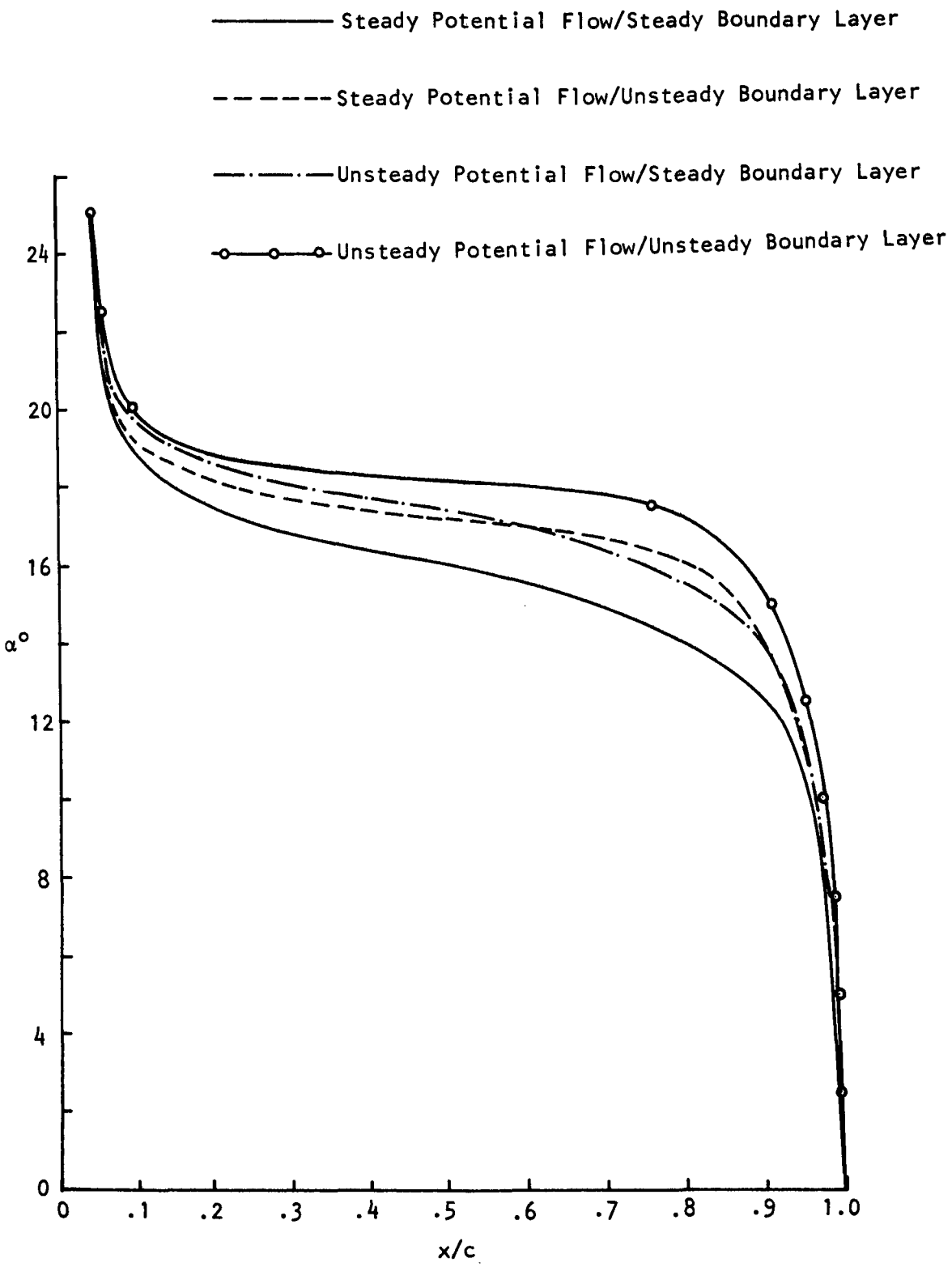

Figure 9. Forward Movement of Flow Reversal Point with Increasing Incidence, $c\dot{\alpha}/U_\infty = .02$

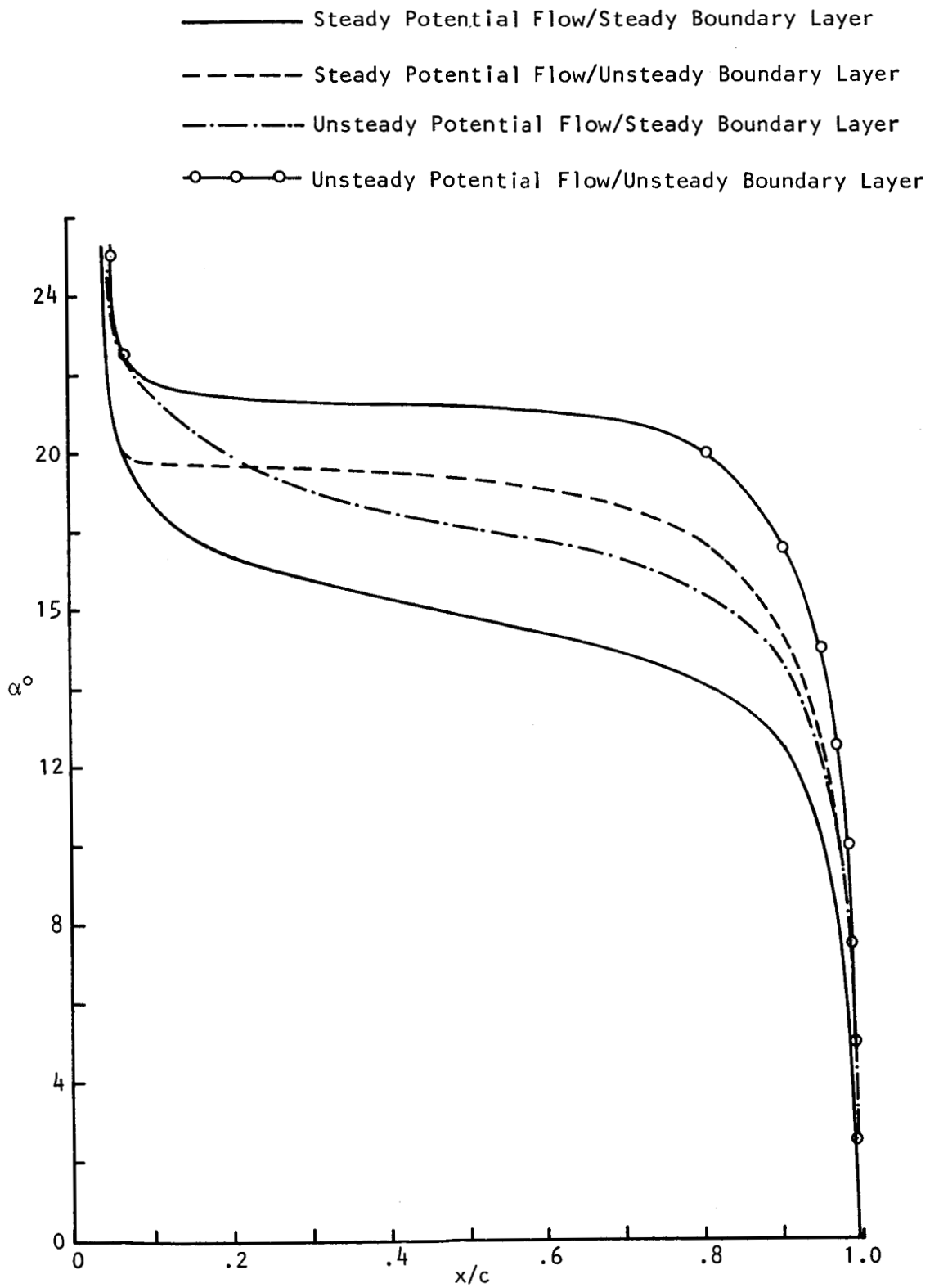

Figure 10. Forward Movement of Flow Reversal Point with Increasing Incidence, $c\dot{\alpha}/U_\infty = .04$

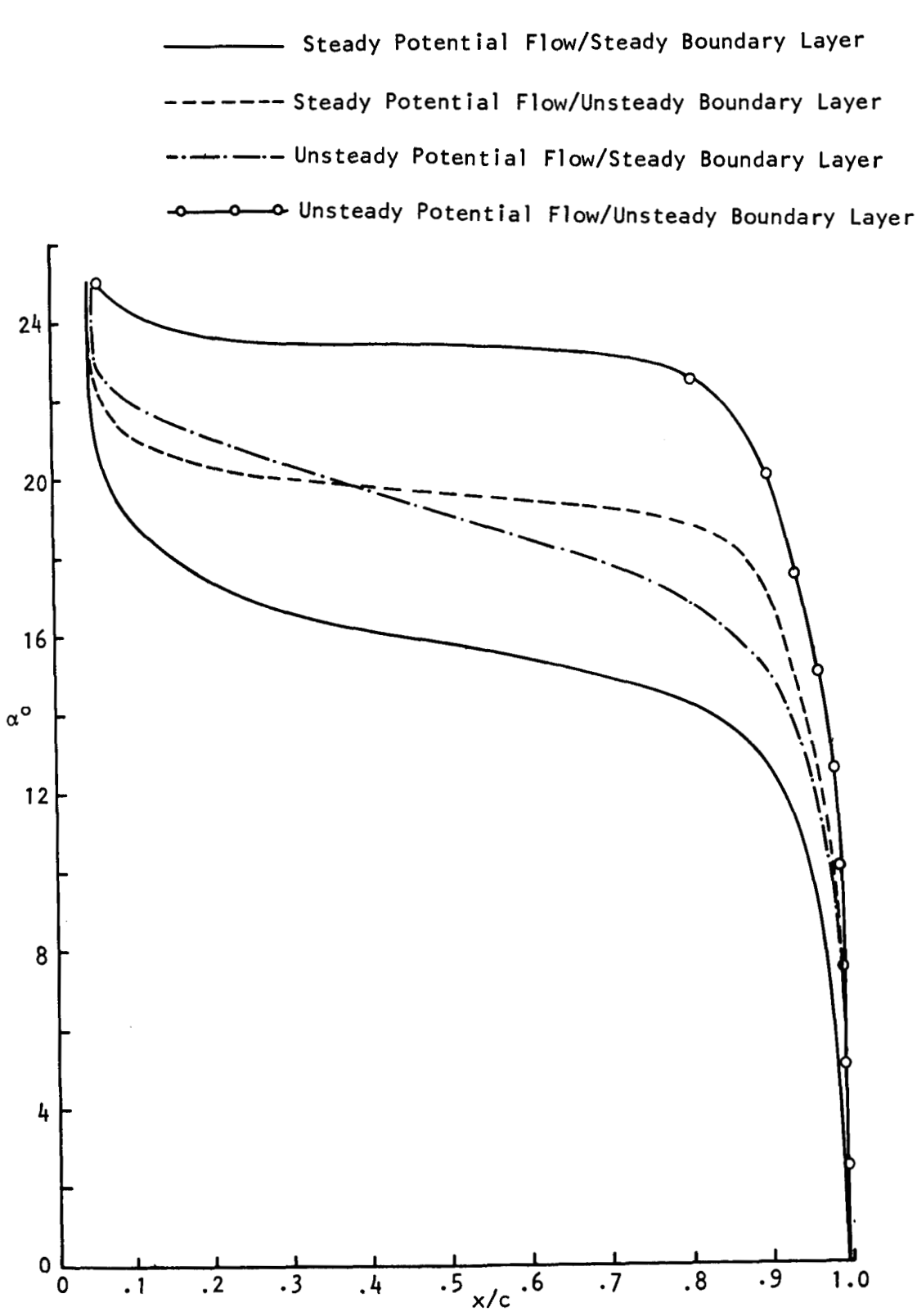

Figure 11. Forward Movement of Flow Reversal Point with Increasing Incidence, $c\dot{\alpha}/U_\infty = .06$

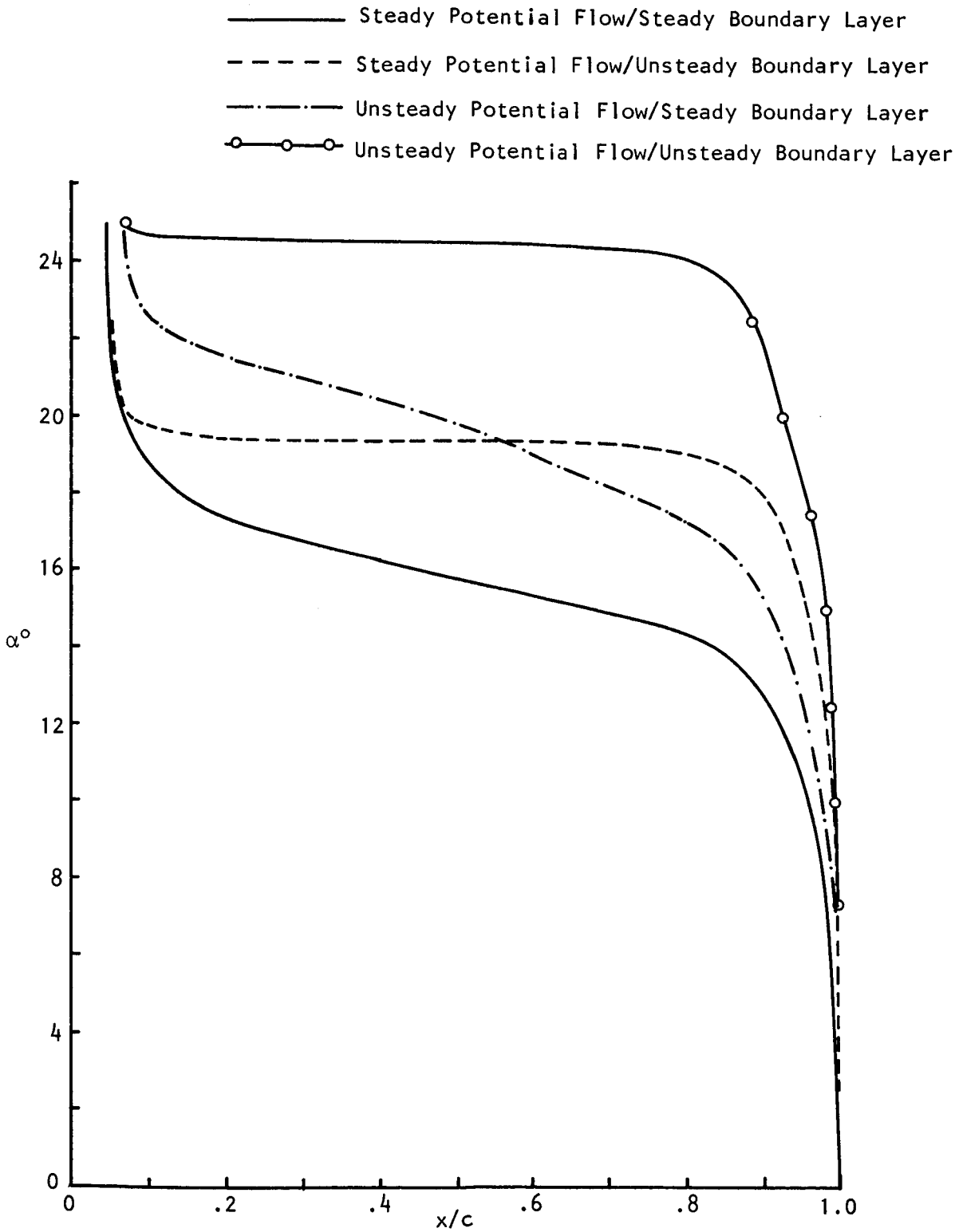

Figure 12. Forward Movement of Flow Reversal Point with Increasing Incidence, $c\dot{\alpha}/U_\infty = .08$

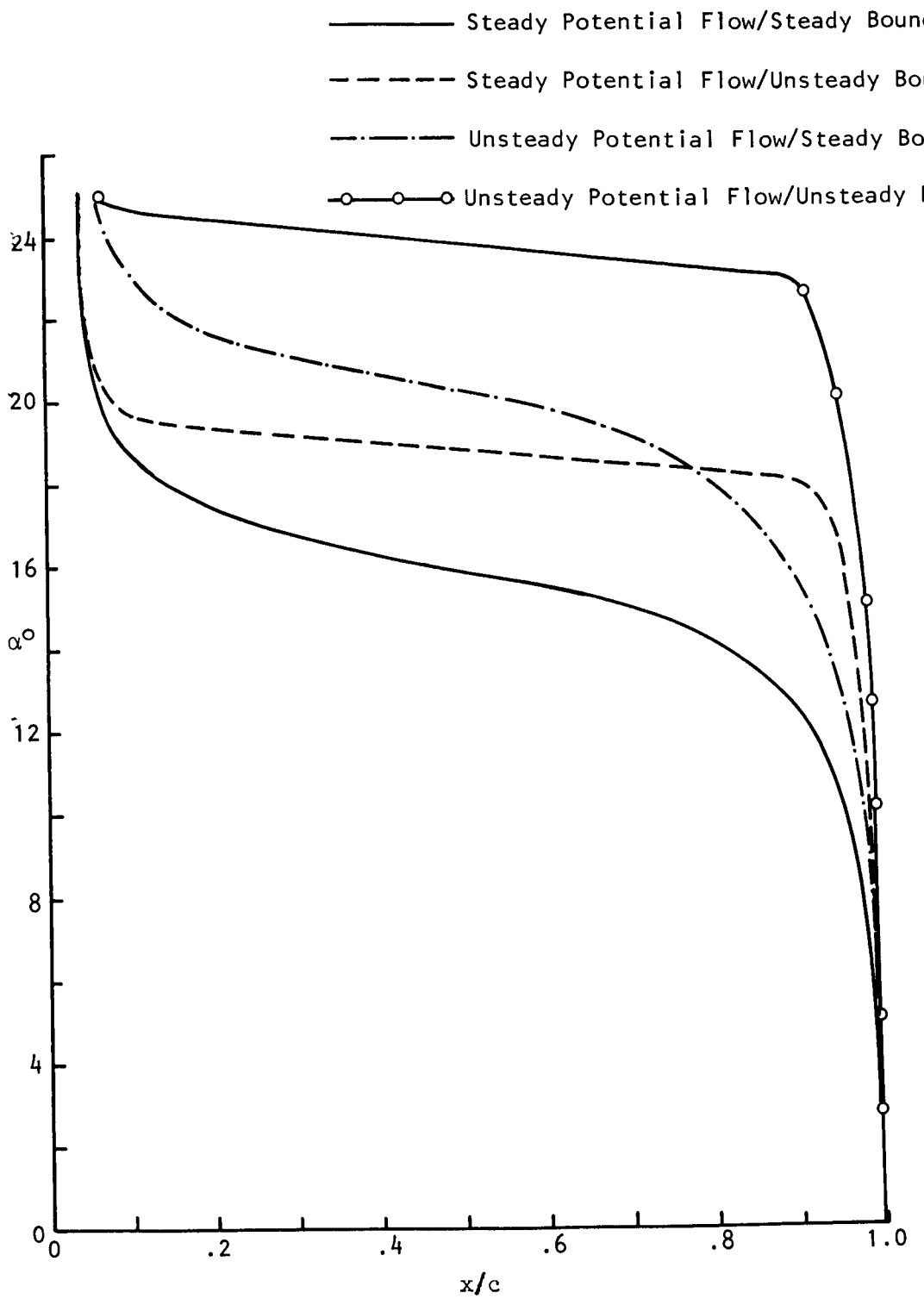

Figure 13. Forward Movement of Flow Reversal Point with Increasing Incidence, $c\dot{\alpha}/U_\infty = .10$

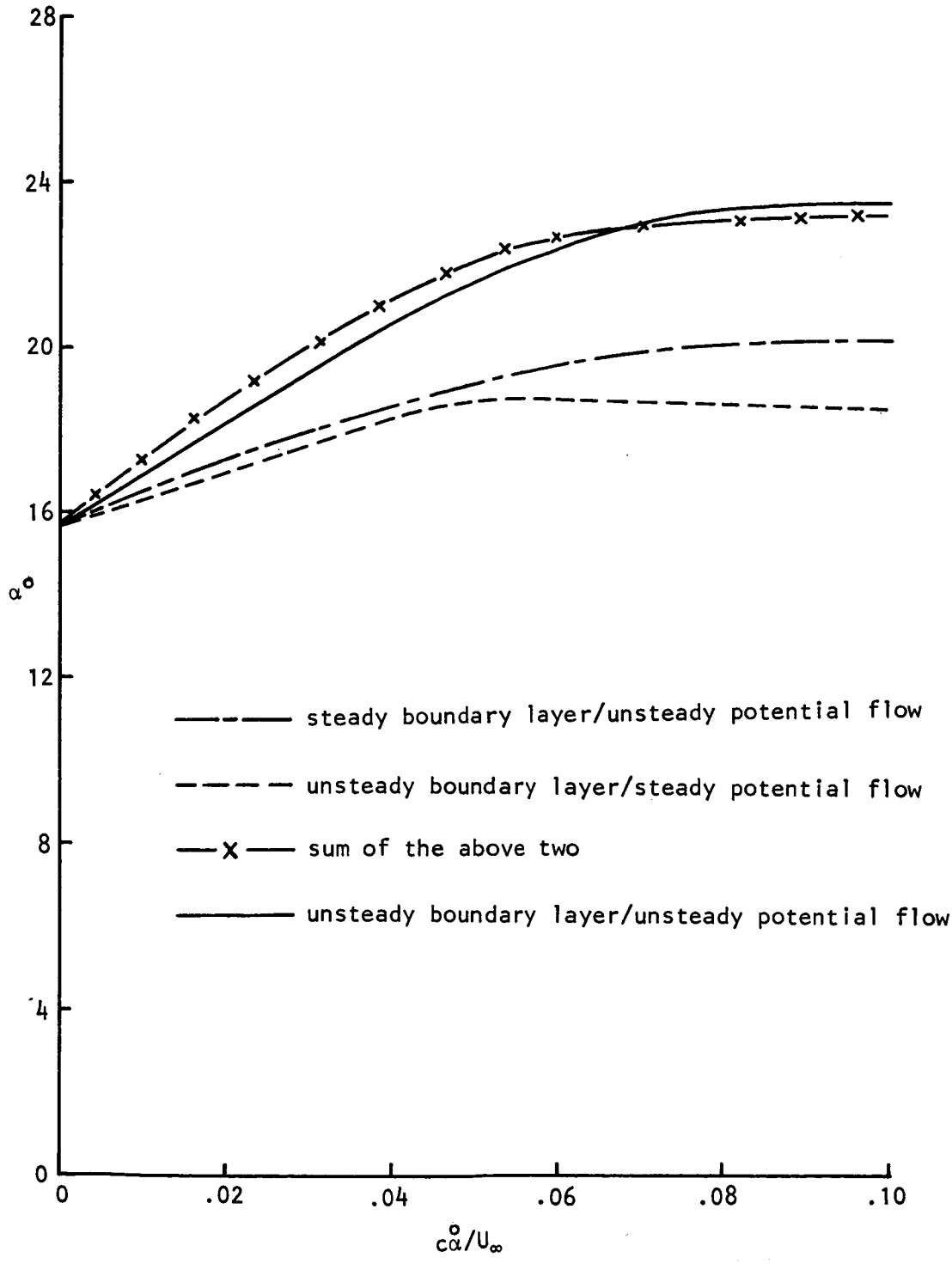

Figure 14.
Increase in Incidence for Flow Reversal at .5c Due to Pitch Rate

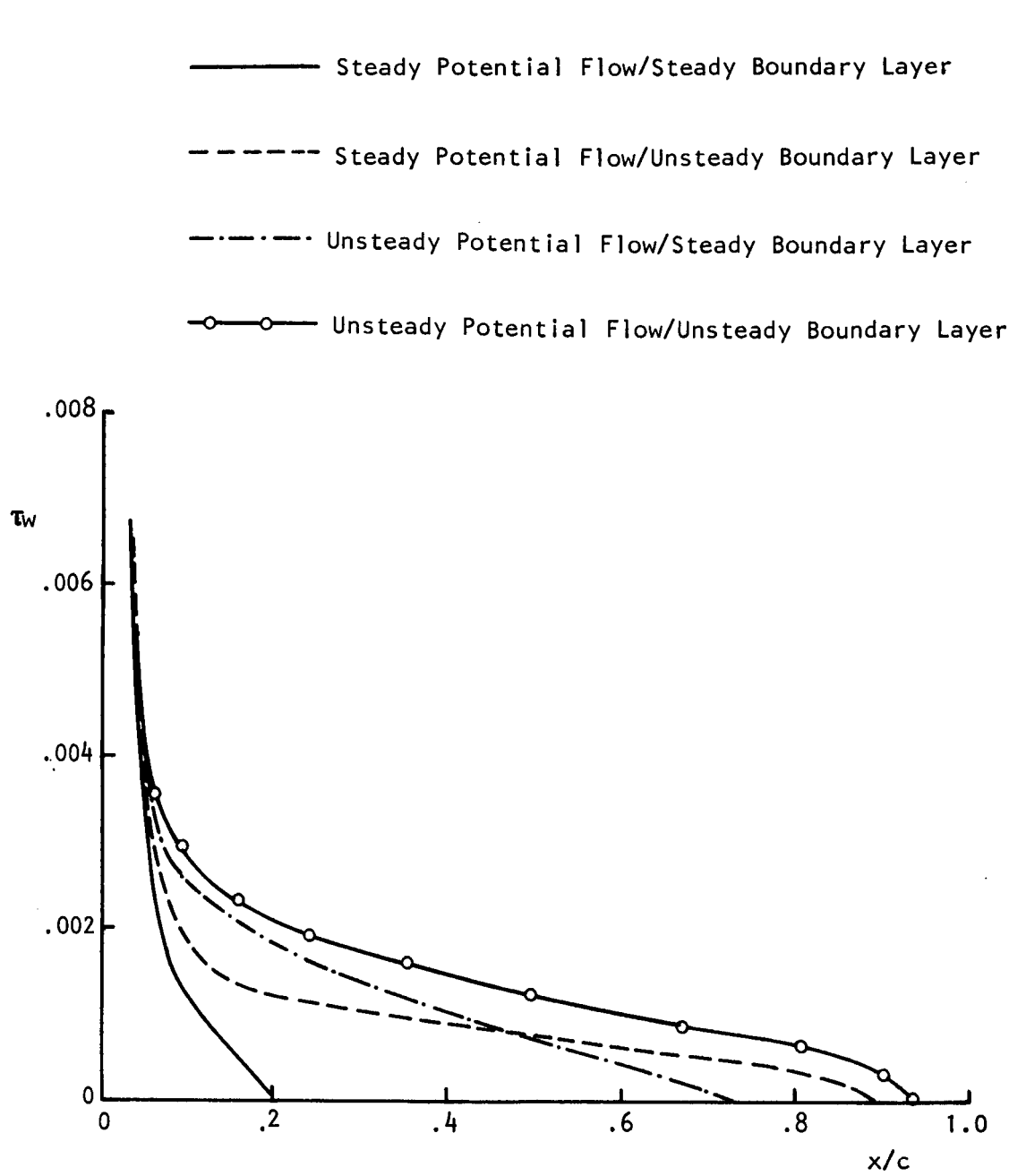

Figure 15. Wall Shear Stress Versus Chordwise Position at $\alpha = 17.5$ and $c\dot{\alpha}/U_\infty = .06$

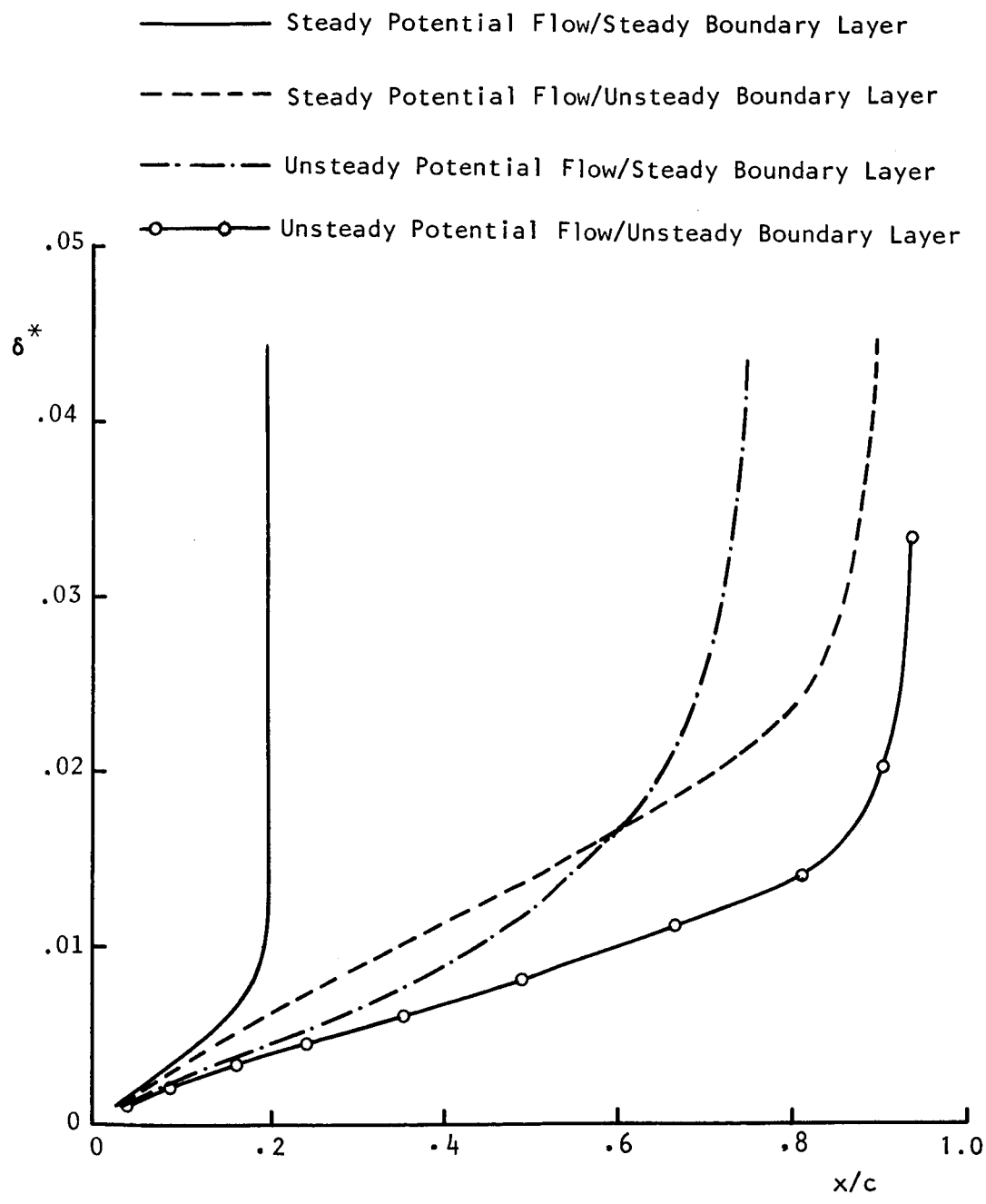

Figure 16. Displacement Thickness Versus Chordwise Position at $\alpha = 17.5$ and $c\dot{\alpha}/U = .06$

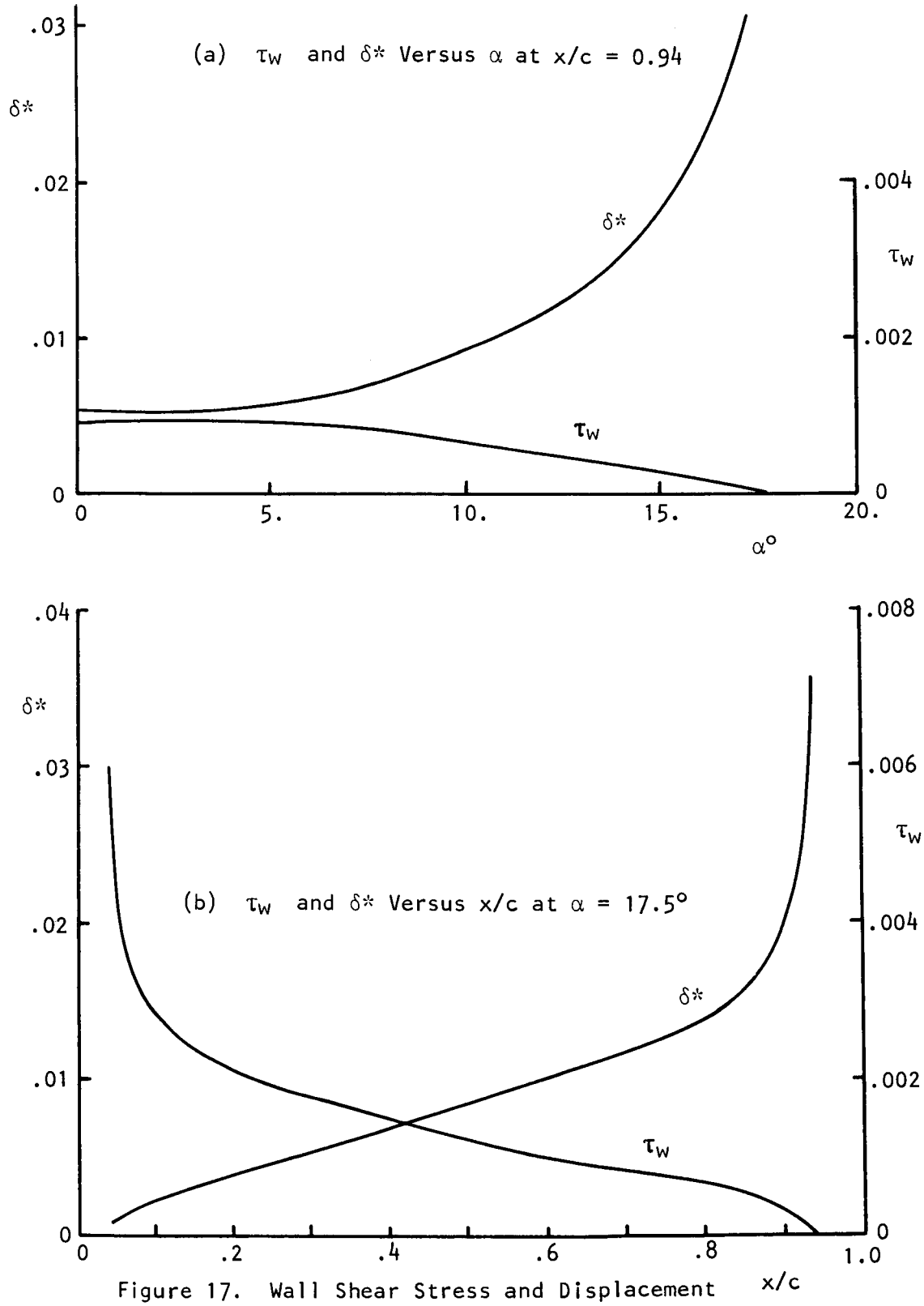

Figure 17. Wall Shear Stress and Displacement Response for the Fully Unsteady, $c\dot{\alpha}/U_\infty$ = .06

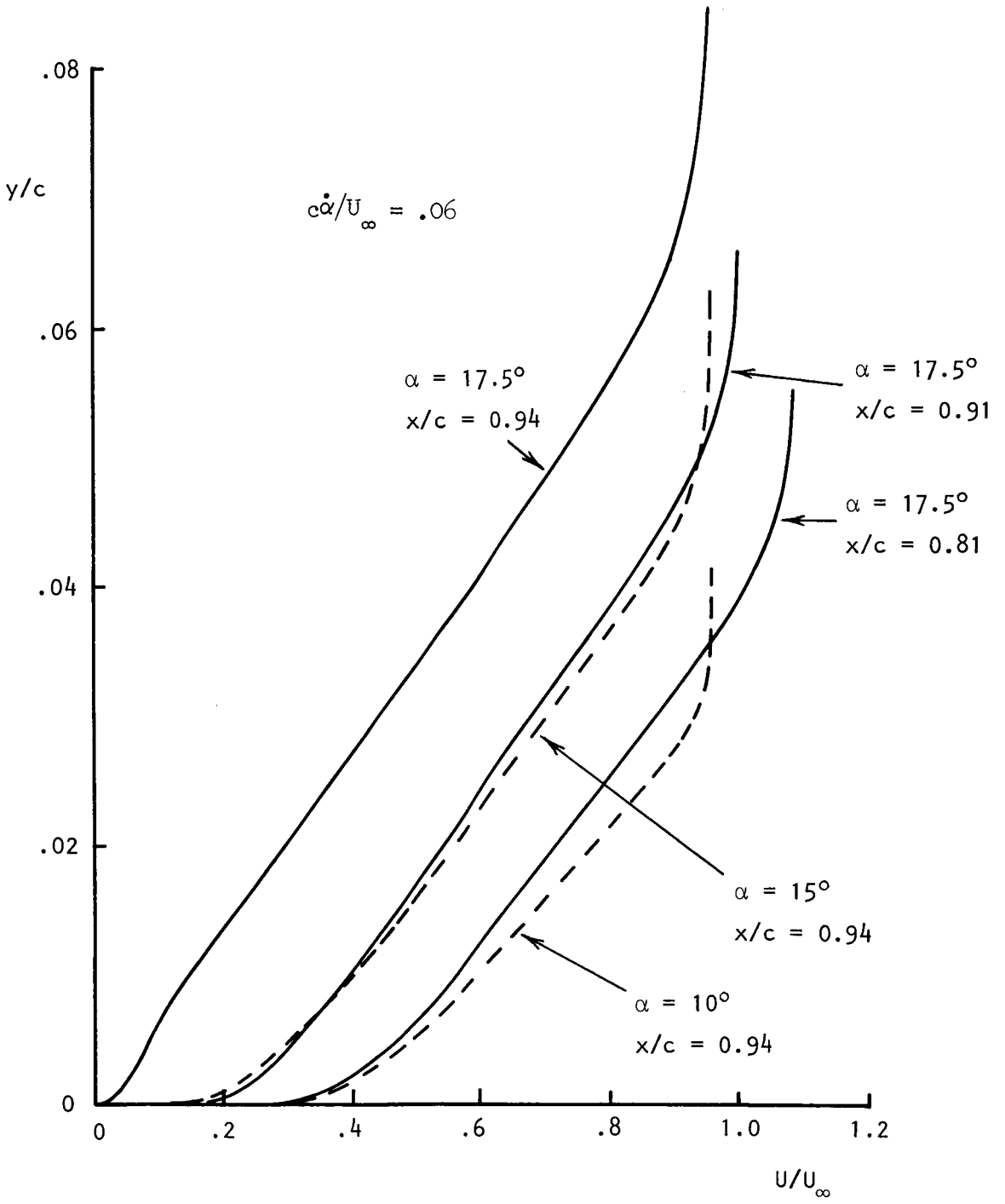

Figure 18. Approach to Flow Reversal:

Velocity Profiles at Selected Chordwise Stations and Incidences

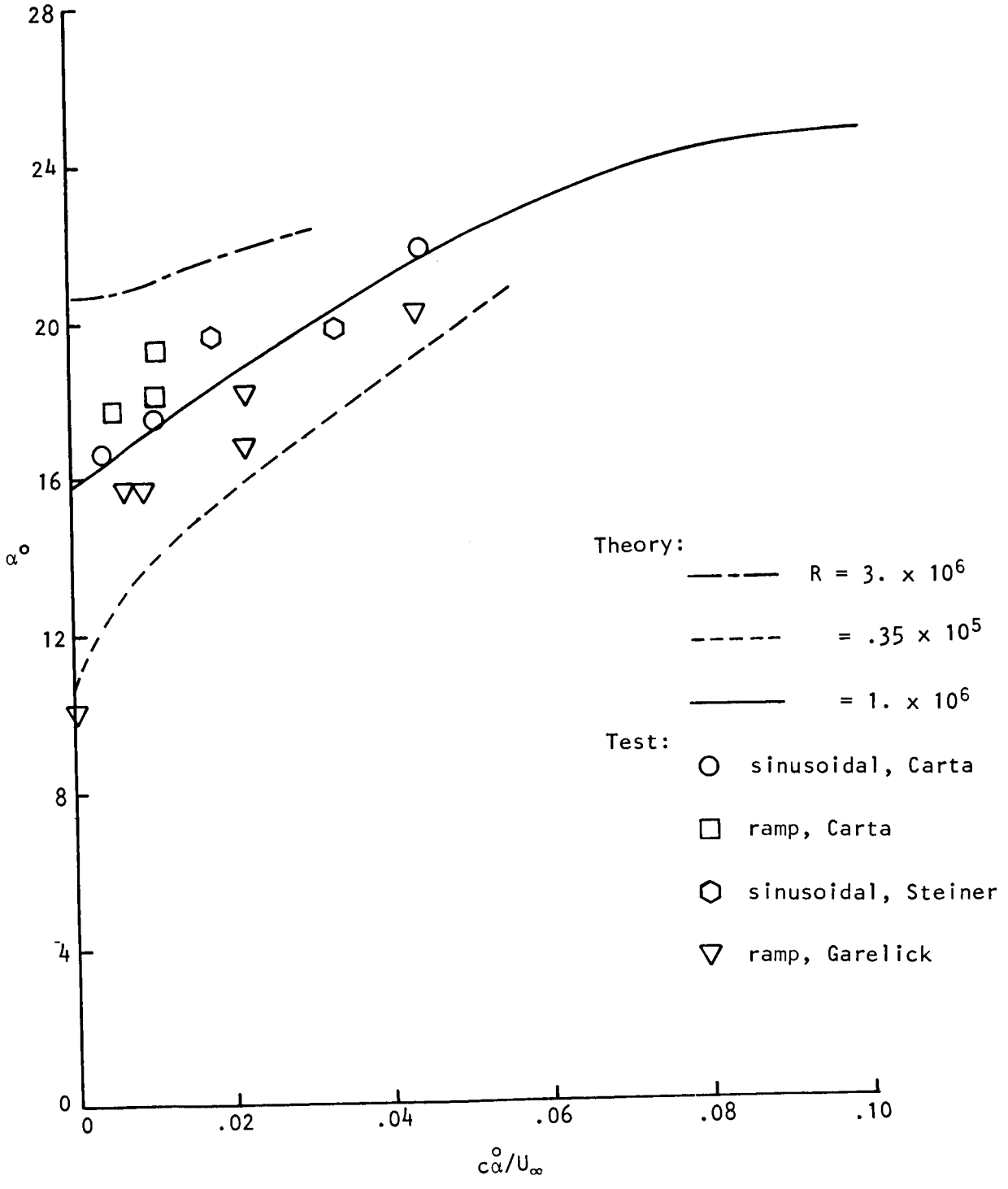

Figure 19. Comparison with Experiment